Supramolecular Chemistry and Molecular Self-Assembly

M2 – Ecole polytechnique - Université Paris-Saclay
France

Supramolecular chemistry in diagnosis and therapeutic chemistry

Outline

1. Thermodynamic and kinetic aspects
2. Calyxarenes, dendrimers and other examples
3. Supramolecular chemistry in diagnosis and therapeutic chemistry
4. Supramolecular chemistry in the environment
5. Discussion

Artificial cells

Nature is full of complex constructions designed to encapsulate molecules within a defined space.

A clathrin

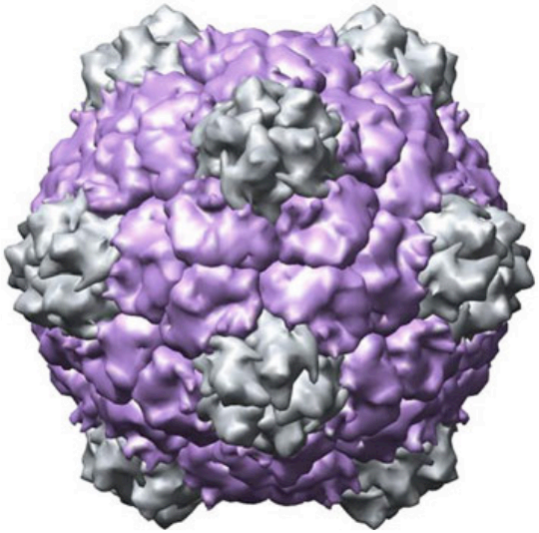

A capsid virus

A protein vault

Molecular cages: coordination chemistry

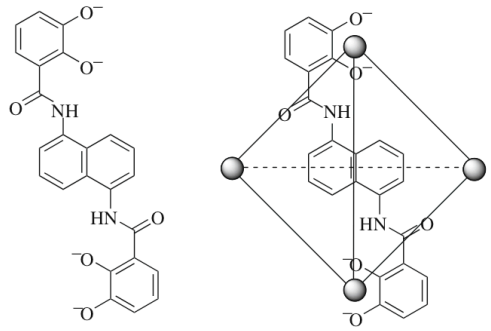

Raymond, *Angew. Chem. Int. Ed.*, **2006**, 83

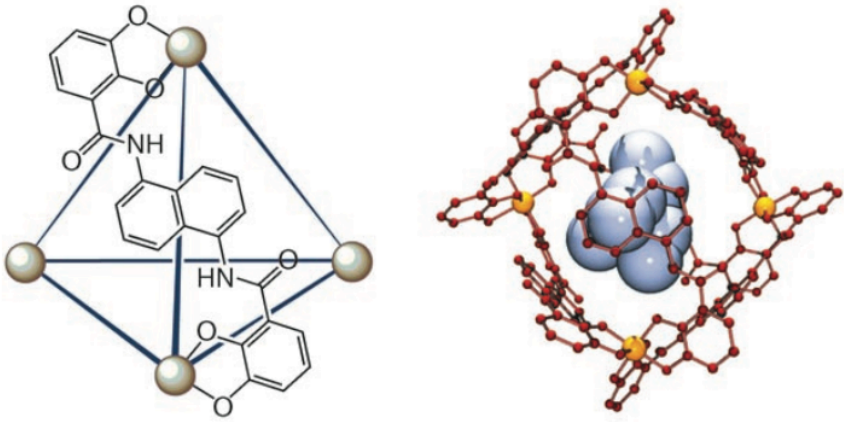

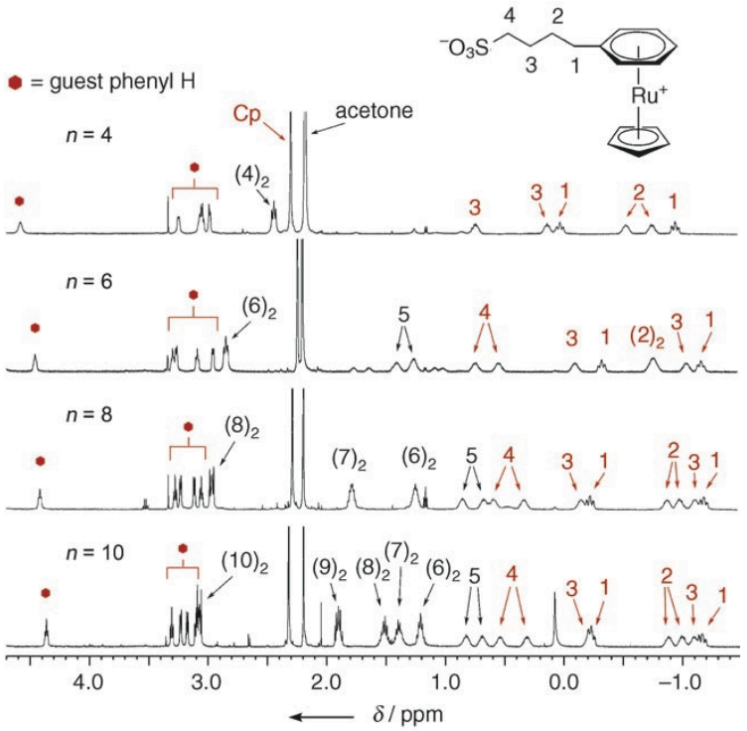

Figure 1. Left: Schematic structure of the M_4L_6 tetrahedral cluster which illustrates the structure of L^{4-} and its coordination to the metal-ion vertices. Right: Illustration of the host–guest complex $[Et_4N{\subset}Ga_4L_6]^{11-}$ based on the X-ray structure coordinates, with a Et_4N^+ guest shown in blue.

Molecular cages: coordination chemistry

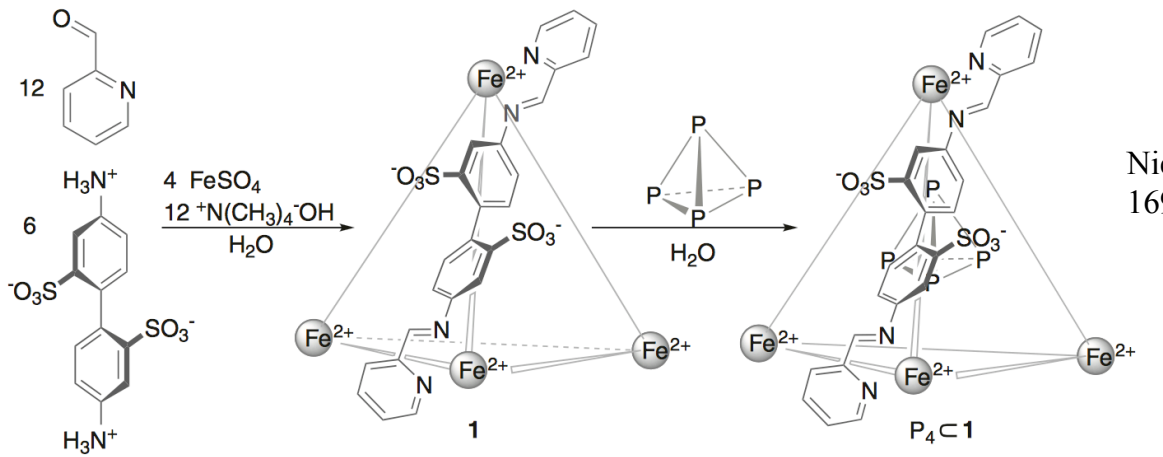

Nietsche, *Science,* **2009**, 1697

Fig. 1. Synthesis of tetrahedral cage **1** and subsequent incorporation of P_4.

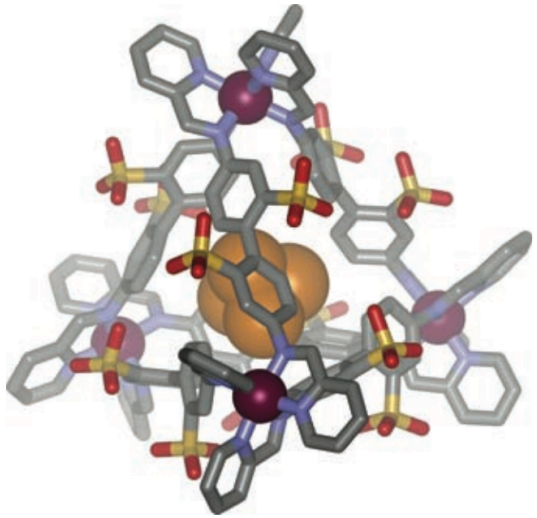

Fig. 2. Crystal structure of P_4⊂**1**. Solvent molecules, counterions, and hydrogen atoms are omitted for clarity. Fe, violet; N, blue; C, gray; O, red; S, yellow; P, orange.

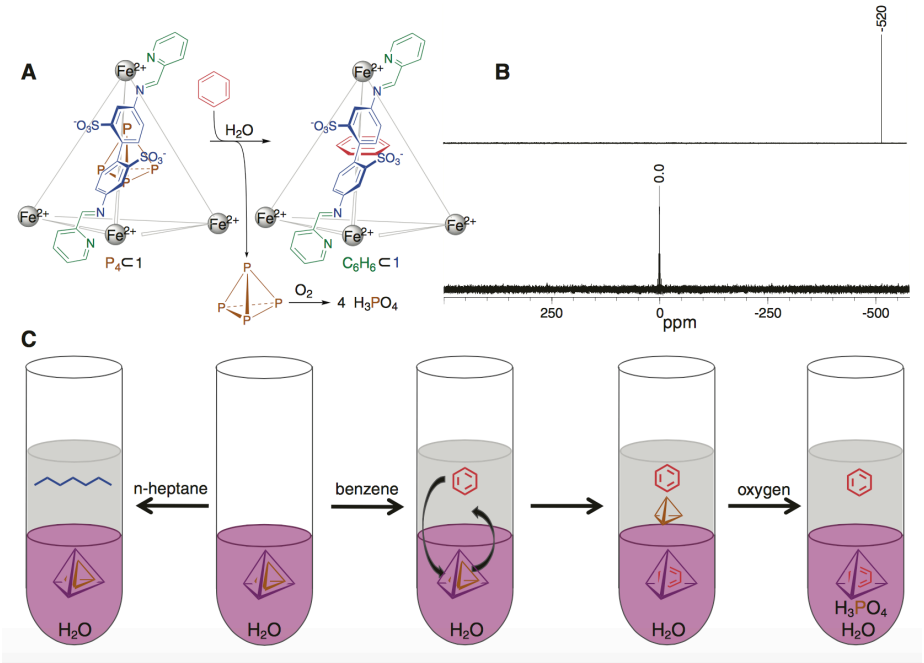

Supramolecular enzyme mimics: cytochrome models

Neumann, *J. Am. Chem. Soc.*, **1989**, *111*, 2900

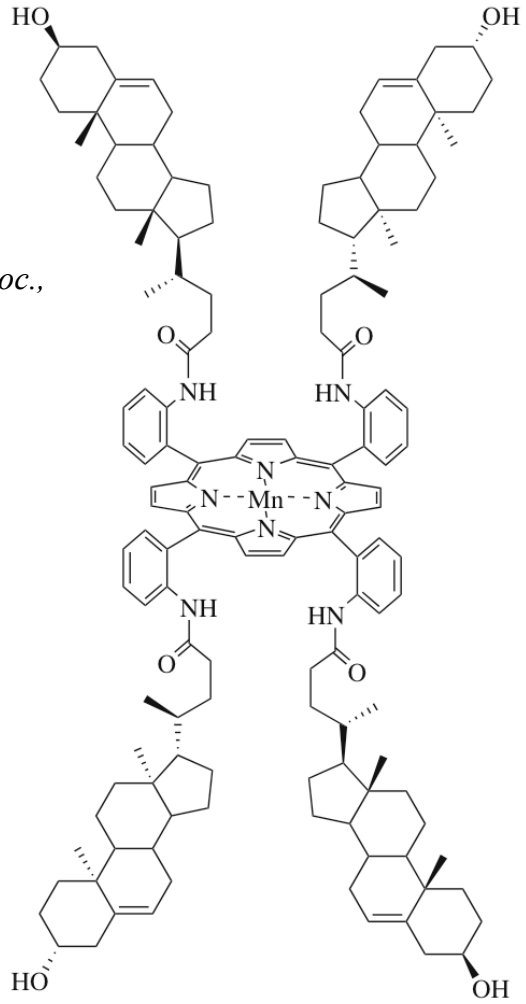

Fig. 4.10 Cytochrome model complexes [22, 23]

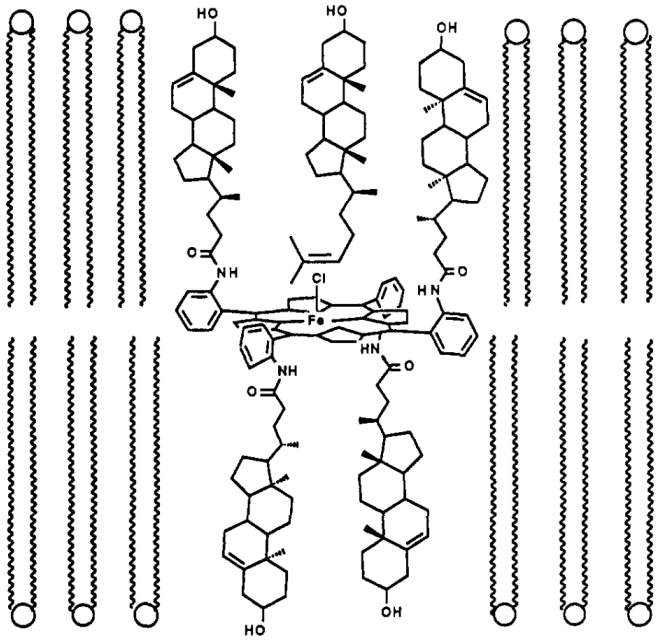

1

Figure 1. Idealized drawing of molecular bilayer assembly of chloro-[$\alpha,\beta,\alpha,\beta$-*meso*-tetrakis[*o*-((3$\beta$-hydroxy-5-cholenyl)amido)phenyl]-porphyrinato]iron(III) (Fe^{III}(ChP)Cl), desmosterol, and phospholipid.

When introduced to vesicles the complex buried itself in the membrane and, once flavoprotein pyruvate oxidase and ethylbenzene were added, generated acetophenone.

Supramolecular enzyme mimics: cytochrome models

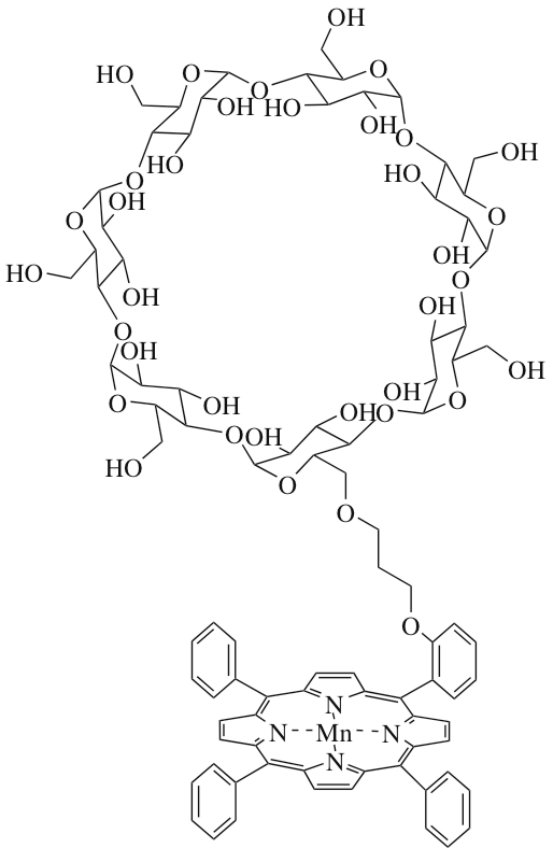

Breslow, *Angew. Chem. Int. Ed.*,**2000**, *39*, 2692

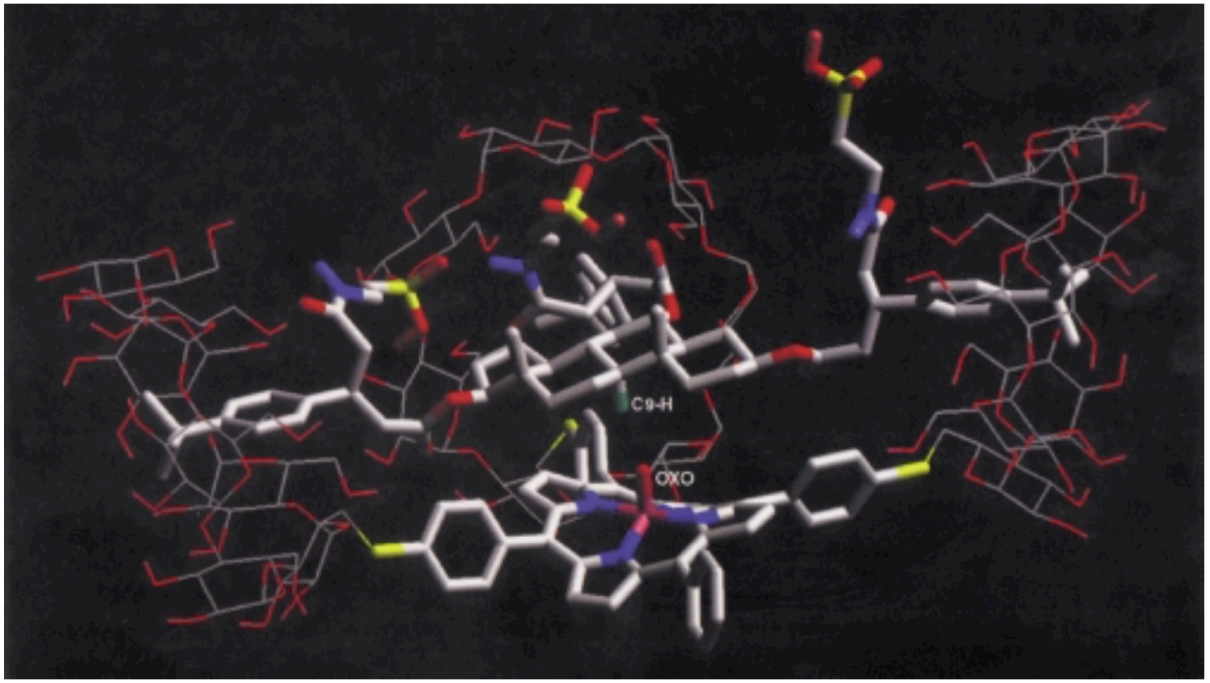

Figure 2. The computed structure of the complex of triply bound substrate **6** with catalyst **1**, showing that the oxygen atom added to the Mn atom of **1** is in a lateral position to attack the axial H atom on C-9 of **6**, as observed. For details of the calculational method, which differs from that in Figure 1, see Experimental Section. For clarity the one cyclodextrin not involved in substrate binding is deleted from the figure, and those binding the substrate are shown with thin lines.

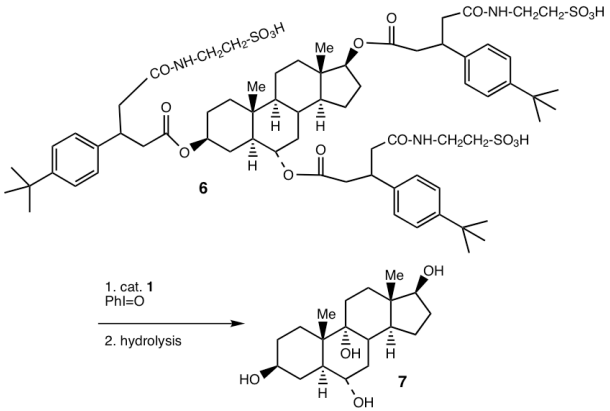

Scheme 2. Catalyst **1** converts a triply bound substrate to the 9α-hydroxy derivative.

Supramolecular enzyme mimics: cytochrome c oxidase

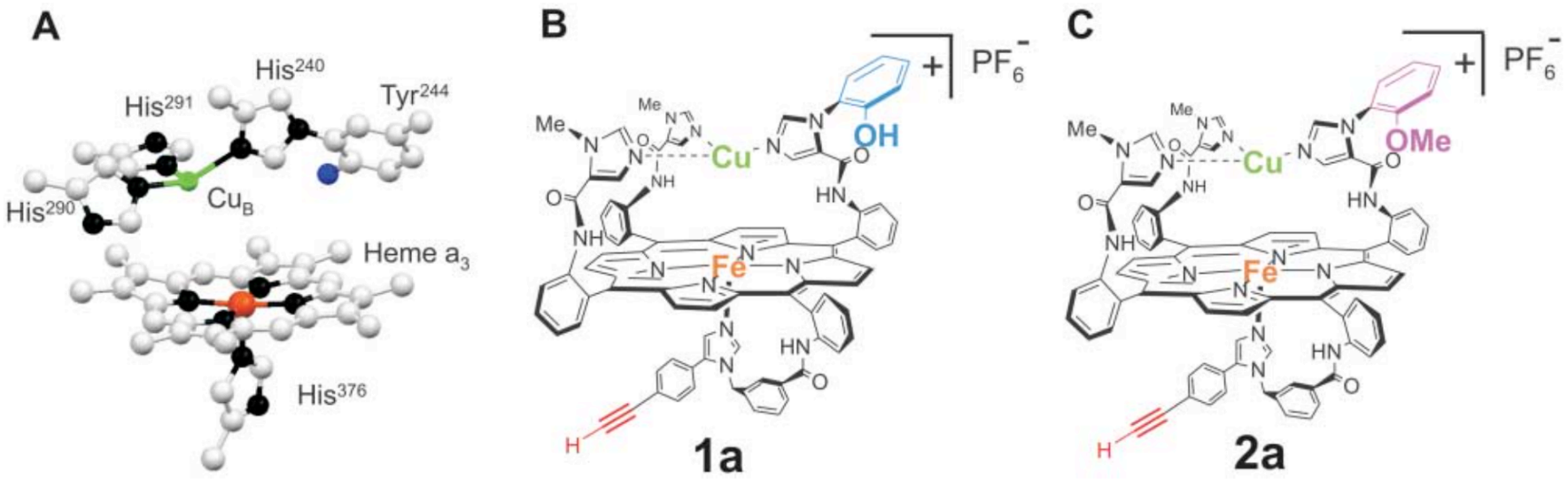

Fig. 1. (**A**) Crystal structure of the active site of CcO from the bovine heart (*13*). (**B**) Model **1a** reproduces the key elements of the active site of CcO. (**C**) Model **2a**, in which the phenol is masked as a methyl ether. Model **2a** can be treated with dilute acid to yield the iron-only model (**2b**), which is not shown.

Cytochrome c oxidase mimics have long been a goal because they catalyse the reduction of dioxygen to water without the generation of other reactive oxygen species.

X-Ray crystallography revealed that the active site consisted of an iron-haem complex with an adjacent copper cation bound by three histidines, in the expected motif, and a nearby tyrosine group. The importance of tyrosine had been overlooked in many model systems but was introduced as an imidazole substituent by the Collman group

Coleman, *Science,* **2007**, *1565*

Supramolecular enzyme mimics: zinc carboxypeptidase

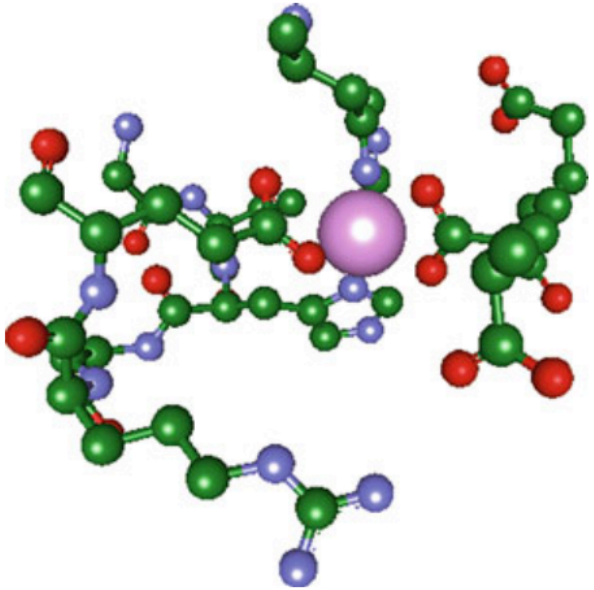

The zinc binding site in carboxypeptidase

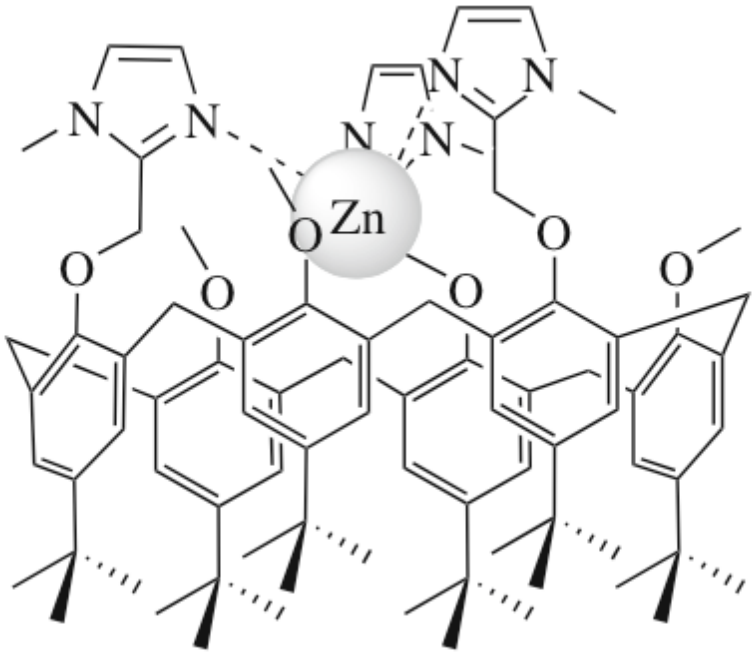

Reinaud, O. *Angew Chem Int Ed Engl*, **2002**, *41*, 1044

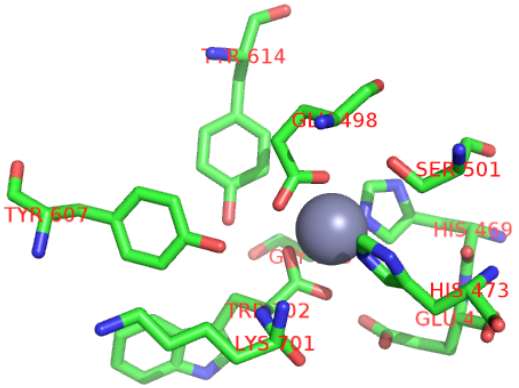

Supramolecular enzyme mimics: carbonic anhydrase

Synthesis and structure of [Zn(OMe)(L)]·[Zn(OH)(L)]·2(BPh_4), L = *cis*,*cis*-1,3,5-tris[(*E*,*E*)-3-(2-furyl)acrylideneamino]cyclohexane: structural models of carbonic anhydrase and liver alcohol dehydrogenase†

Leroy Cronin‡ and Paul H. Walton*
Department of Chemistry, The University of York, Heslington, York, UK YO10 5DD.
E-mail: phw2@york.ac.uk; Fax: +44 1904 432516; Tel: +44 1904 432580

Received (in Cambridge, UK) 13th March 2003, Accepted 2nd May 2003
First published as an Advance Article on the web 29th May 2003

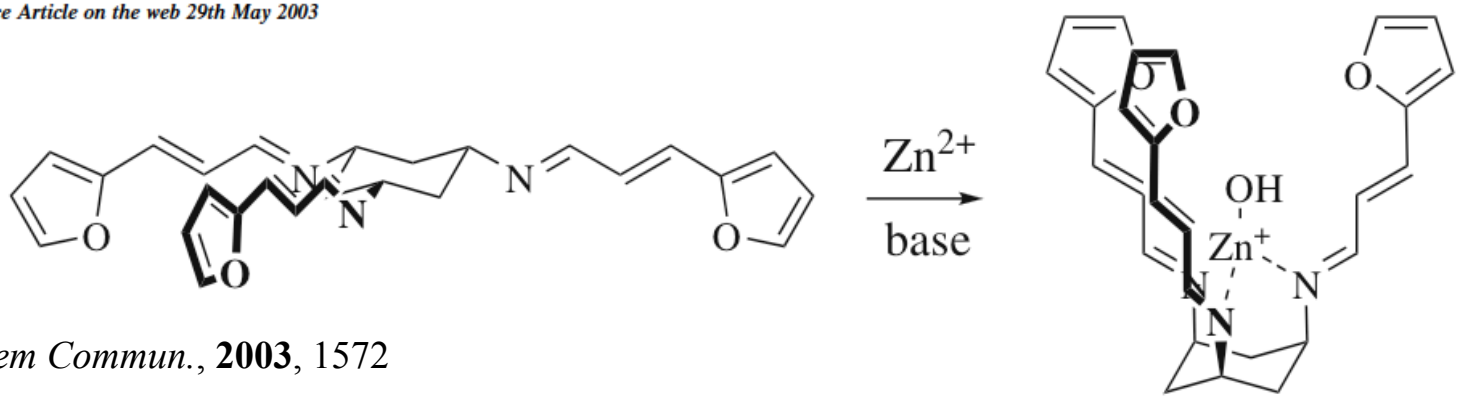

Walton , *Chem Commun.*, **2003**, 1572

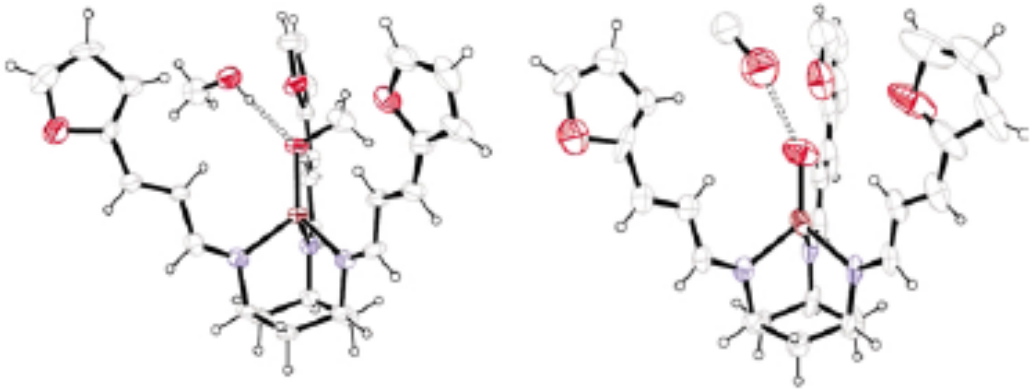

Supramolecular enzyme mimics: ATPase

A crown ether ATPase

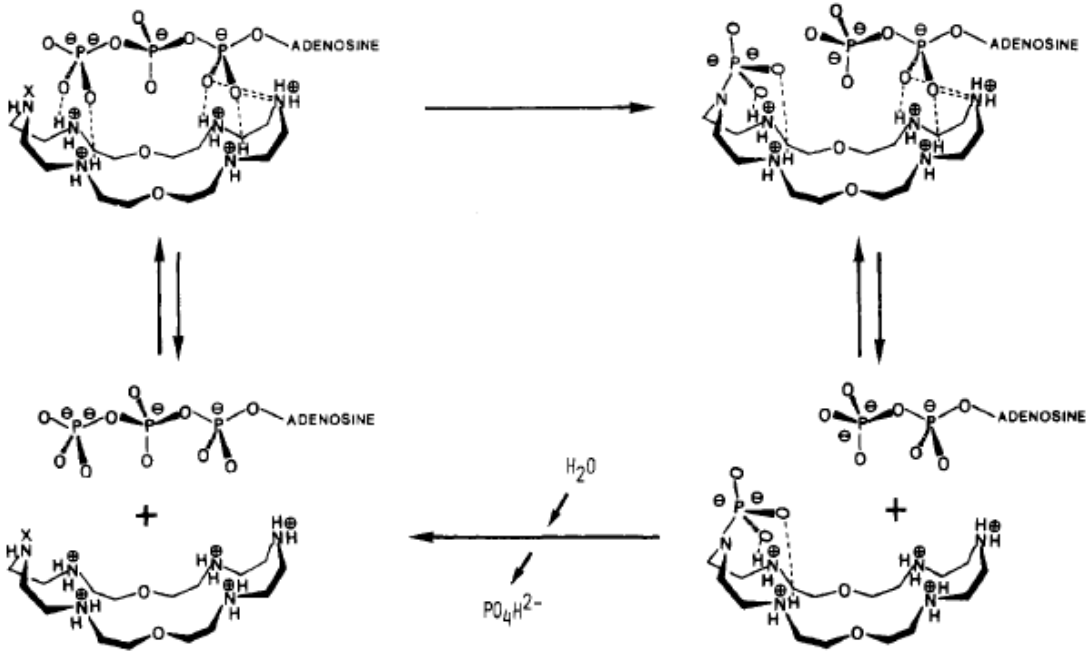

Figure 3. Schematic representation of the catalytic cycle for ATP hydrolysis by the macrocyclic receptor molecule **1** following the nucleophilic pathways. The geometry of the ATP·**1** complex and the binding scheme are hypothetical (see text and ref 11) but compatible with the structures, the dimensions, and the binding-site arrangement of the two partners.

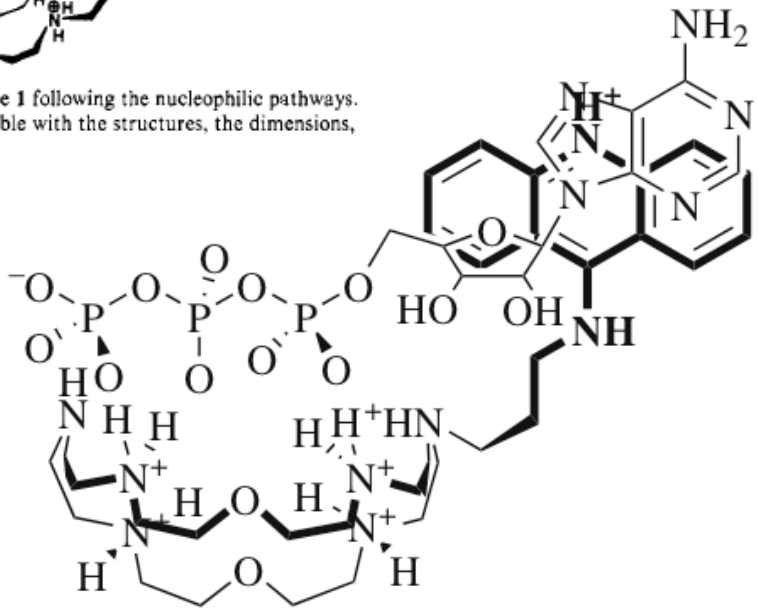

Hosseini, *J Am Chem Soc*, **1987**, *109*, 537

Supramolecular enzyme mimics: Siderophores

Yeast, fungi and bacteria, such as the *Salmonella* genus and *Escherichia coli*, need to sequester iron from aqueous solution. Unfortunately water soluble Fe^{2+} is easily oxidized to Fe^{3+} in air which makes it much less soluble. At concentrations of around 10^{-17} M for free Fe^{3+} in aqueous solution it is essential that every available ion is bound effectively and transported across the cell membrane. This is achieved by siderophores, iron-specific chelating agents that bind Fe^{3+} in an octahedral pocket usually comprising three bidentate catechol or hydroxamate groups

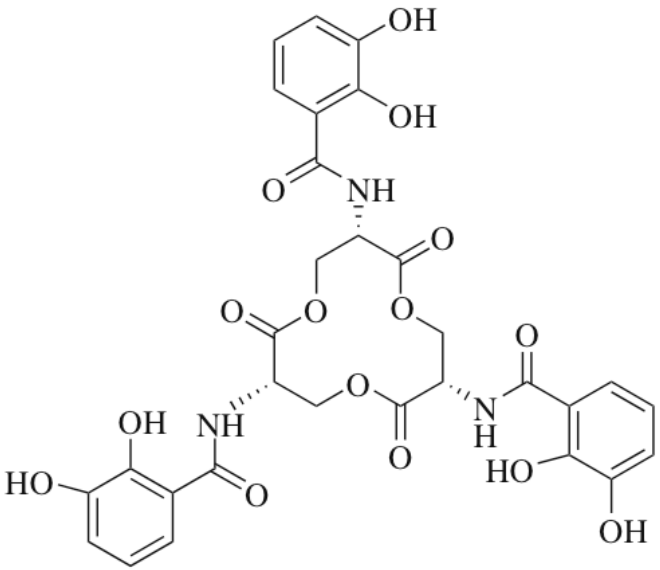

enterobactin

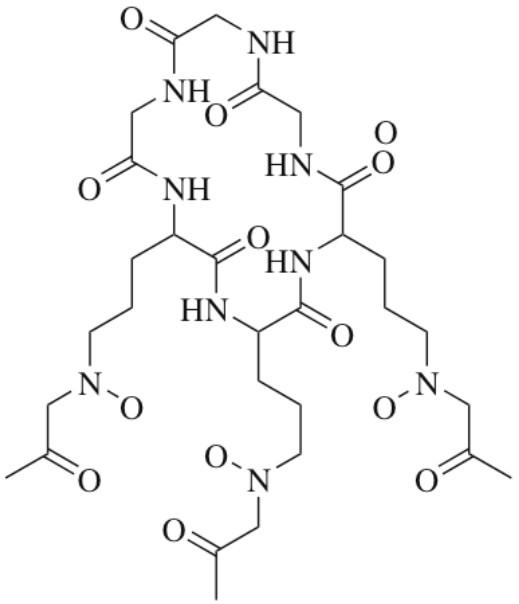

ferrichrome

Supramolecular enzyme mimics: Anion Transport

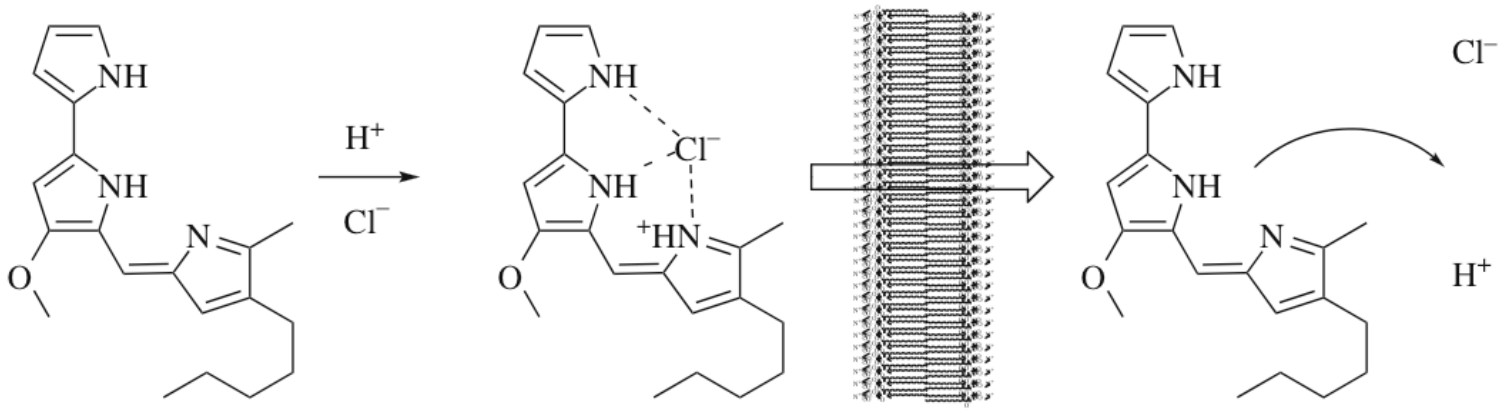

Fig. 5.4 Proton ancd chloride co-transport by prodigiosin

Anions can also be transported across membranes. In Nature, Cl− is transported by prodigiosins which comprise three conjugated pyrrole groups and a lipophilic alkyl tail

Sato T et al., *J Biol Chem,* **1998**, *273*, 21455

Transmembrane Channels: Selectivity and Gating Mechanisms

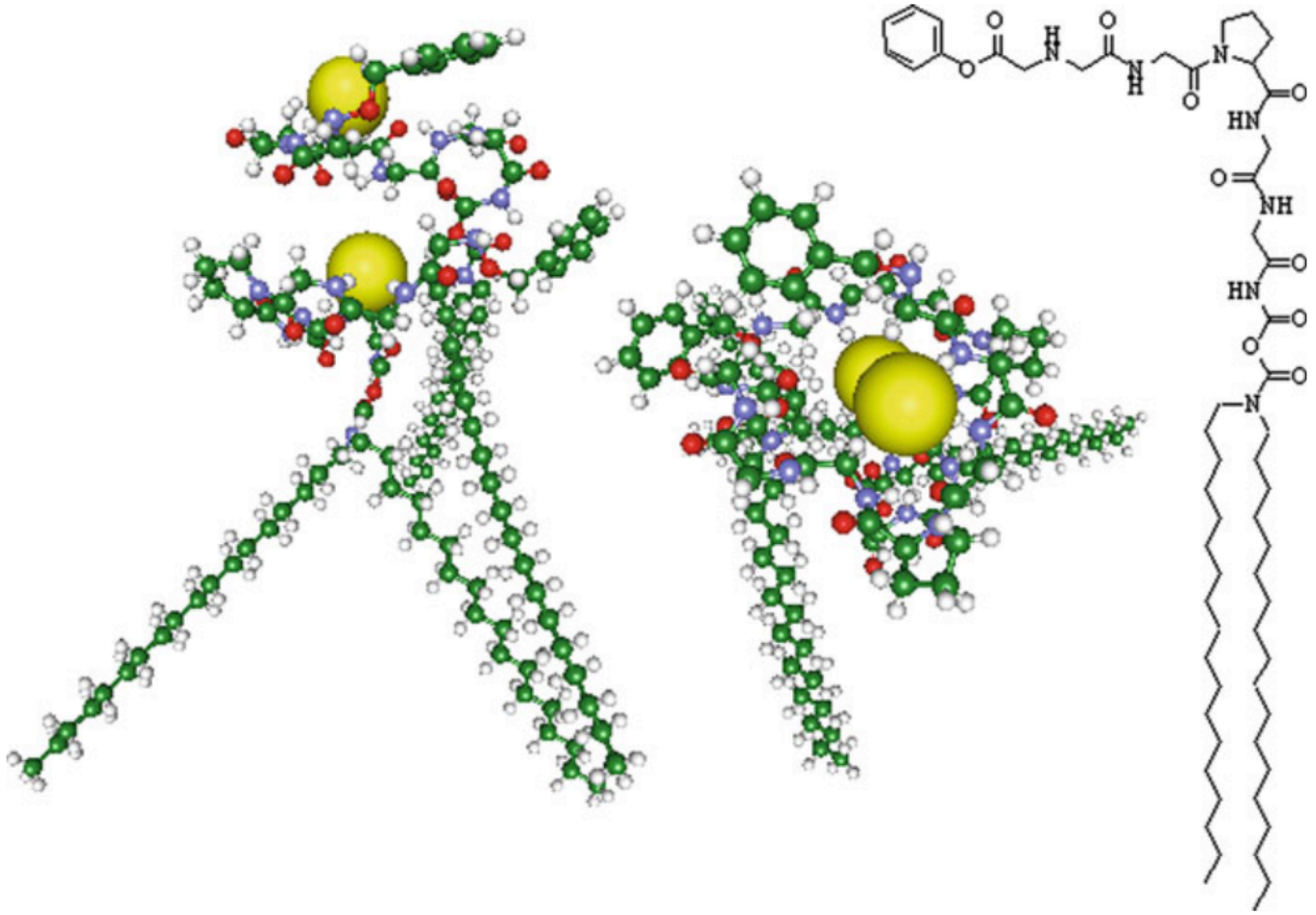

Fig. 5.6 Chloride transport by peptide aggregation in an artificial system [14]

Schlesinger PH et al. *J Am Chem Soc,* **2002**, *124*, 1848

Ion Transport Ionophores and Siderophores

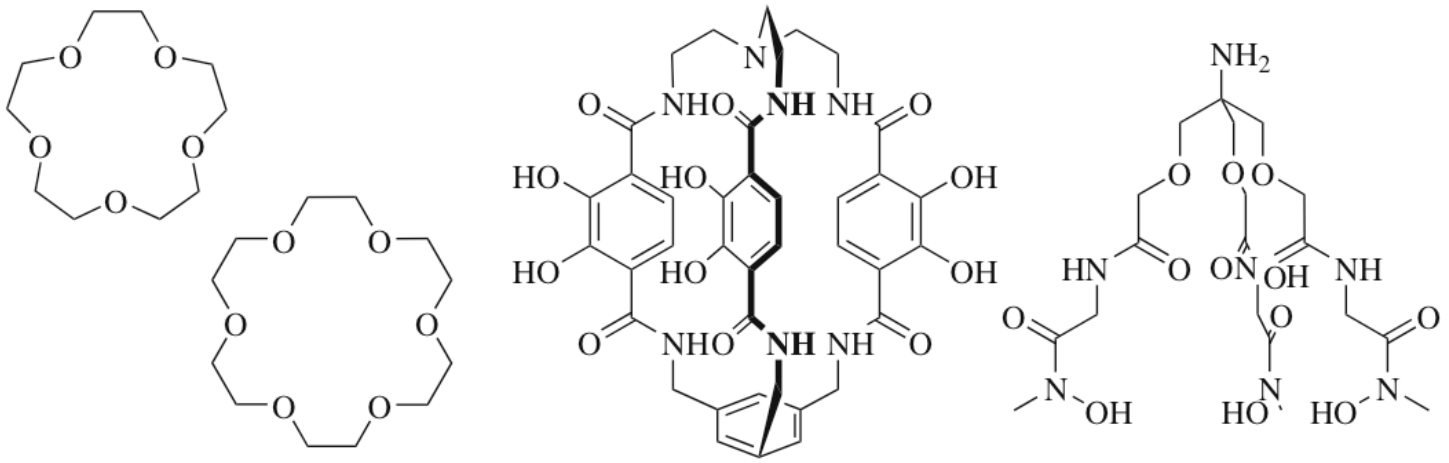

Fig. 5.12 Artificial ionophores and siderophores: (*left* to *right*) Na^+-selective [15]crown-5, K^+-selective [18]crown-6, Fe^{3+}-selective cryptand and podand

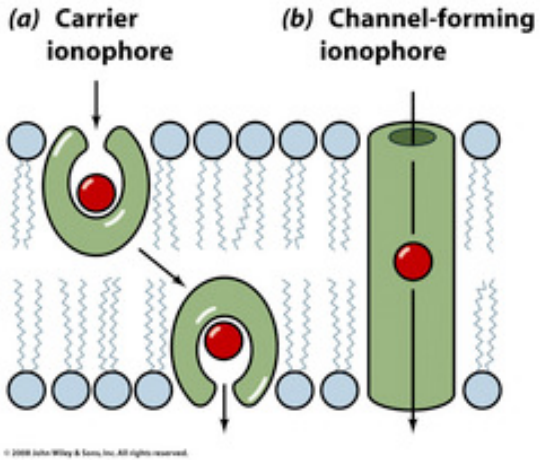

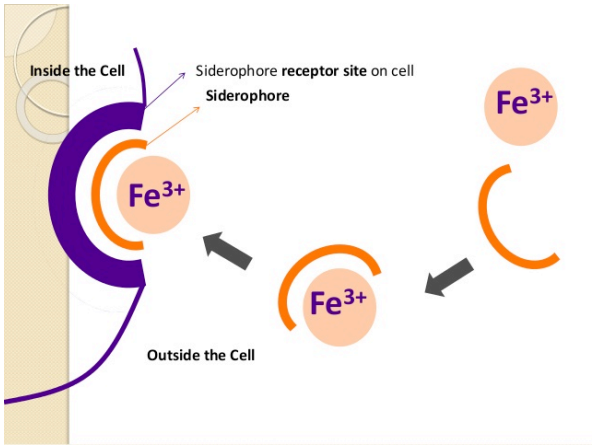

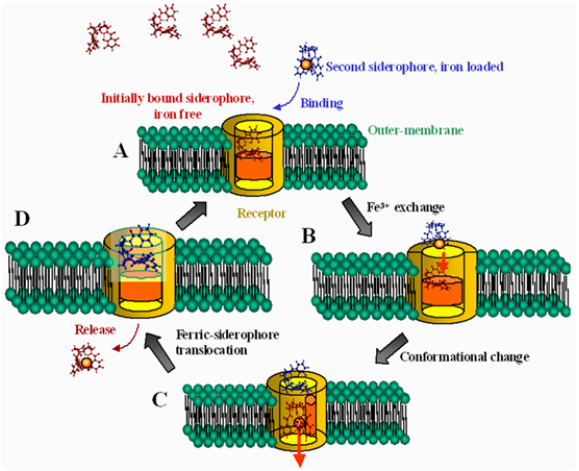

Ken Raymond, Berkeley

Ion Transport: Anion Transport

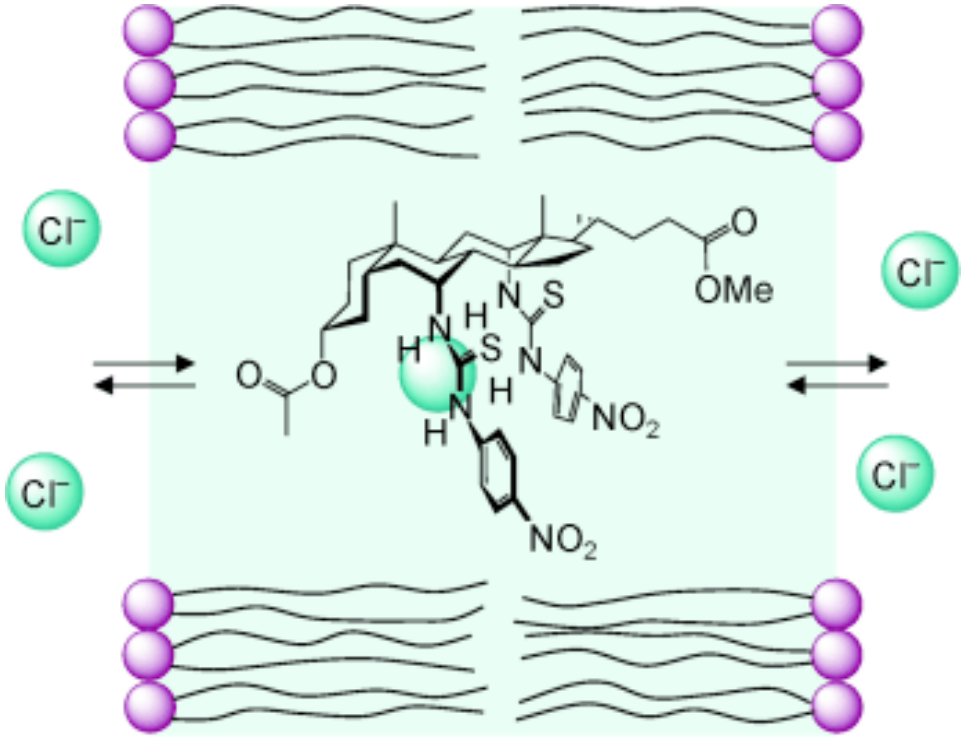

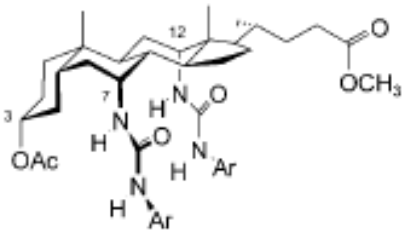

1a: Ar = 4-methoxyphenyl
1b: Ar = 3-methoxyphenyl
1c: Ar = 4-methylphenyl
1d: Ar = phenyl
1e: Ar = 4-nitrophenyl

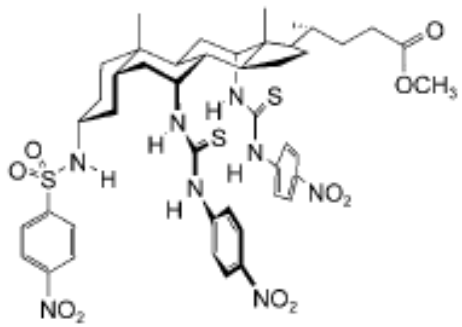

2

McNally BA et al., *Chem Eur J,* **2008**, 14, 9599
Structure-activity relationships in cholapod anion carriers: enhanced transmembrane chloride transport through substituent tuning

Artificial Channel-Forming Peptides

Lear, Masserman, DeGrado, *Science*, **1988**, *240*, 1177

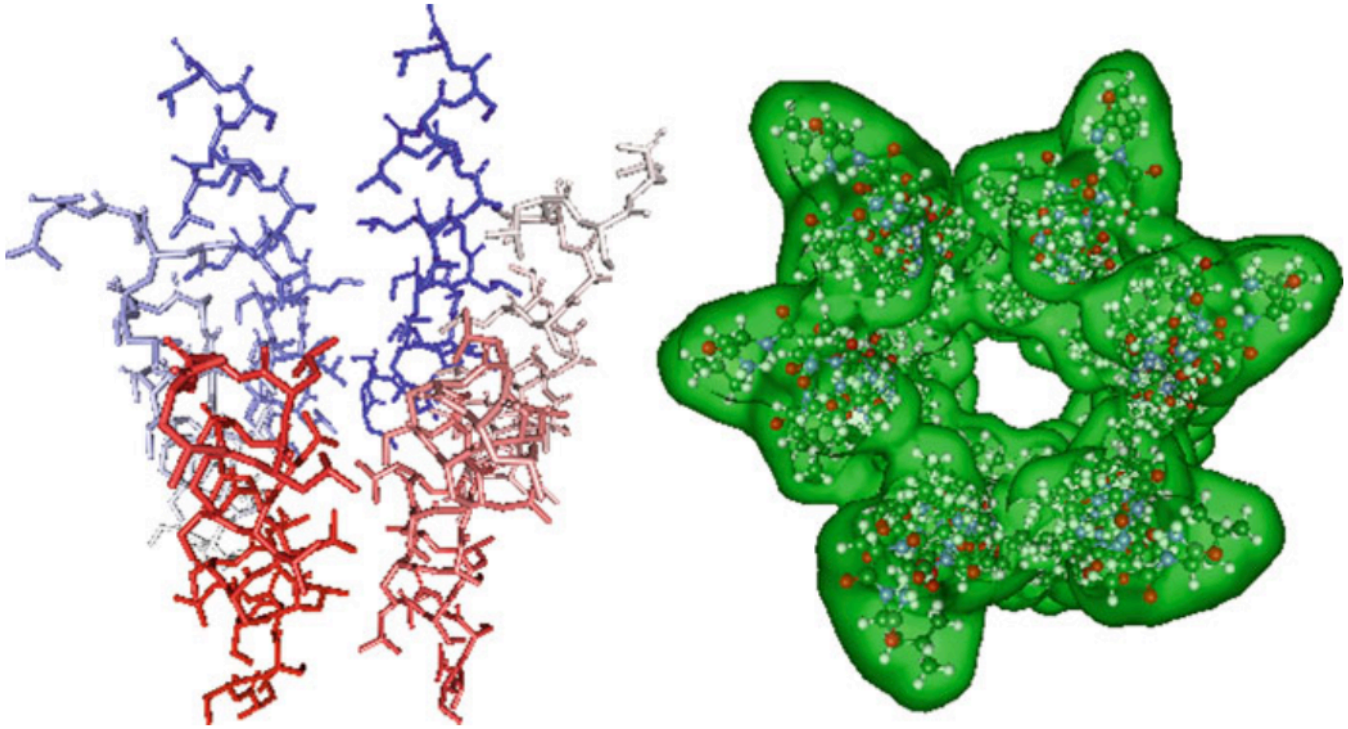

Fig. 5.13 Hexameric transmembrane channels formed by synthetic peptides [42]

A 21-residue peptide, H_2N-(Leu-Ser-Ser-Leu-Leu-Ser-Leu)^3-$CONH_2$, which was designed to be a membrane-sp amphiphilic a-helix, formed well-defined ion channels with ion permeability and lifetime characteristics resembling the acetylcholine receptor. In contrast, a 14-residue version of this peptide, which was too short to span the phospholipid bilayer as an a-helix, failed to form discrete, stable channels. A third peptide, H_2N-(ILu-Ser-Leu-Leu-Leu-Ser-Leu)$_3$-$CONH_2$, in which one serine per heptad repeat was replaced by leucine, produced proton-selective channels. Computer graphics and energy minimization were used to create molecular models that were consistent with the observed properties of the channels.

Artificial Channel-Forming Peptides

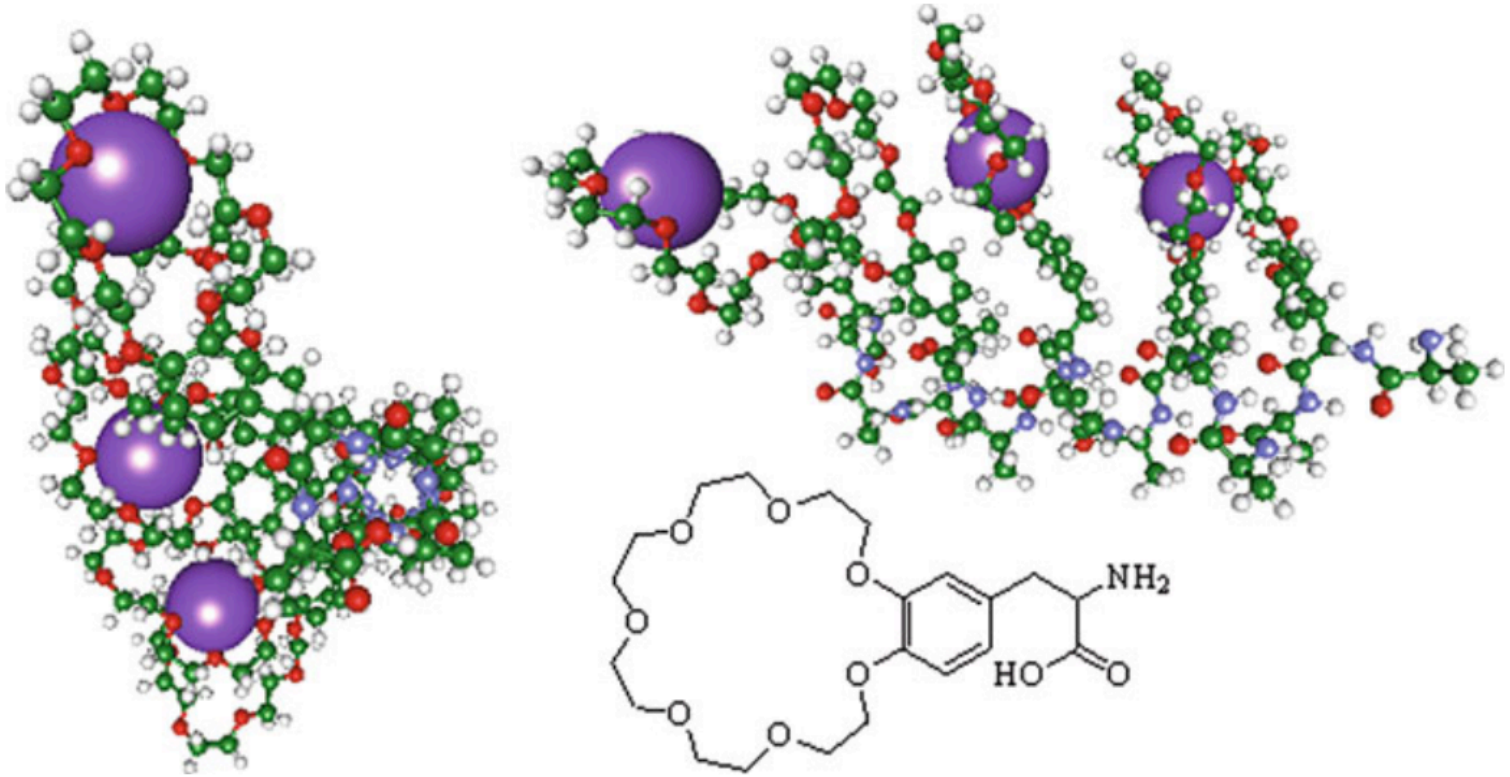

Fig. 5.14 Helical proteins incorporating a crown ether amino acid analogue: a view down the α-helix (*left*) and along the channel (*top*) [43]

Voyer N, Potvin L, Rousseau E, *J Chem Soc Perkin Trans*, **1997**, *2*, 1469

Artificial Channel-Rigid Structures

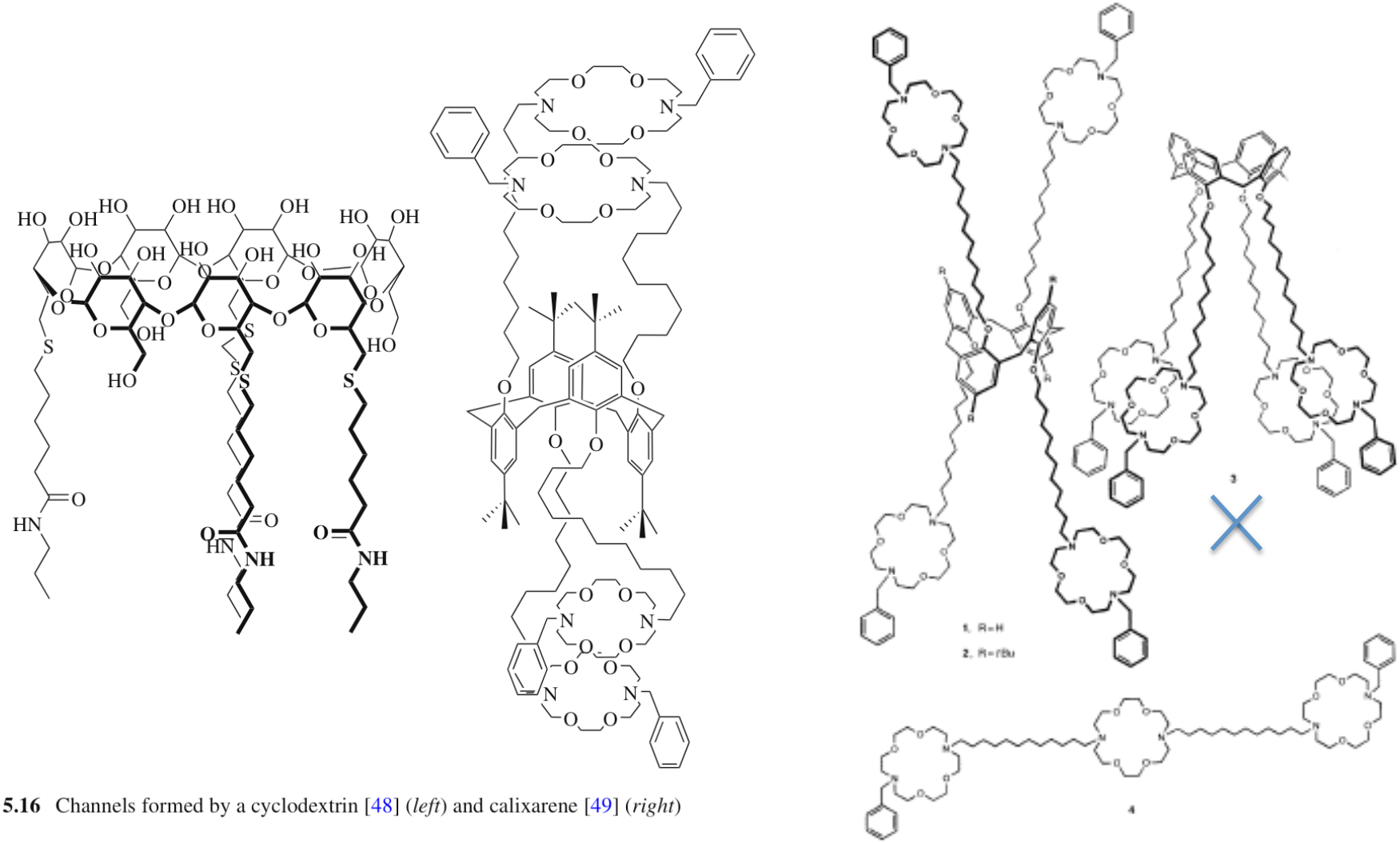

Fig. 5.16 Channels formed by a cyclodextrin [48] (*left*) and calixarene [49] (*right*)

Tabushi I, Kuroda Y, Yokata K. *Tetrahedron Let,* **1982** *23*, 4601
de Mendoza J et al. *Angew Chem Int Ed,* **1998**, *37*, 1534

Diagnosis: Logic Gates

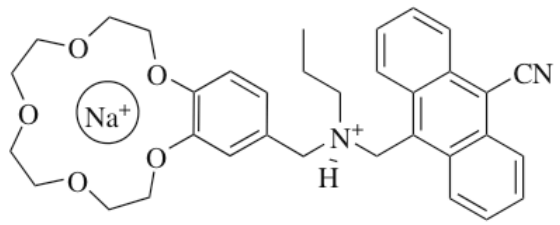

AND gate: $Na^+ + H^+$ = fluorescence

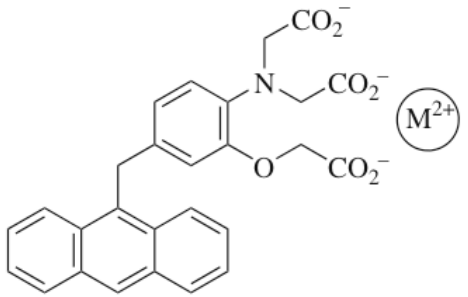

OR gate: any M^{2+} = fluorescence

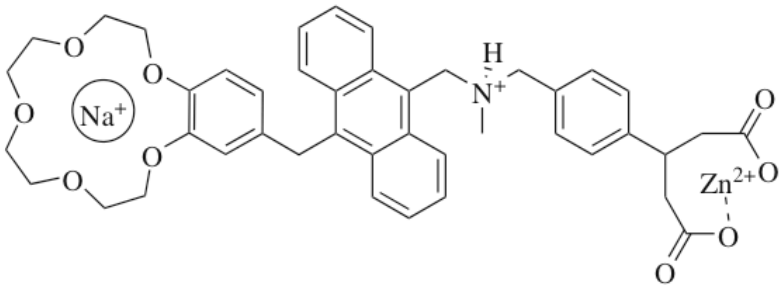

AND gate: $Na^+ + H^+ + Zn^{2+}$ = fluorescence

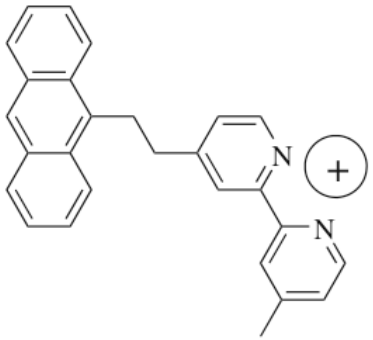

NOR gate: fluorescence quenched by any guest

Fig. 6.5 Examples of logic gates

Diagnosis: Logic Gates

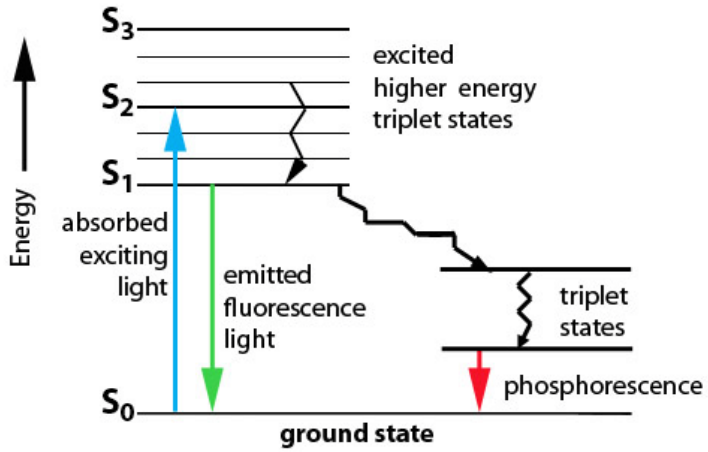

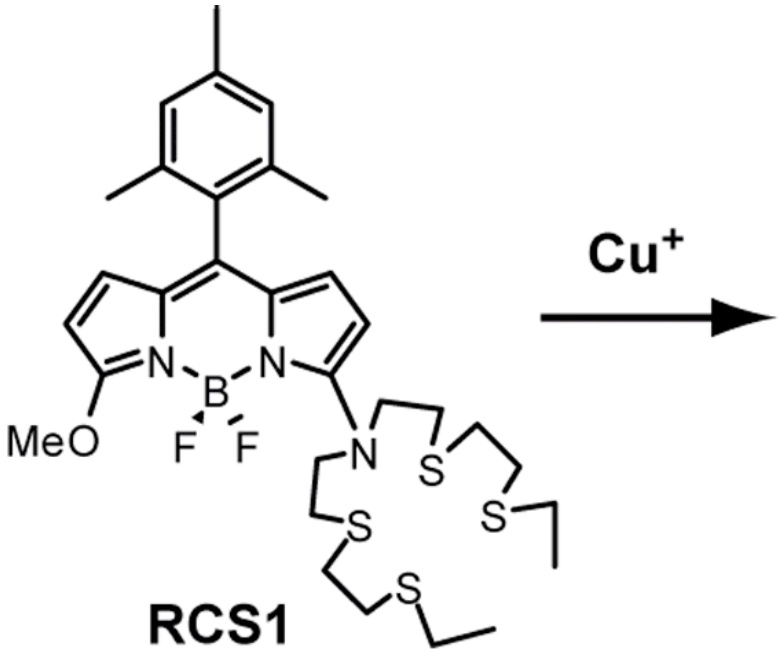

RCS1

Cu^+

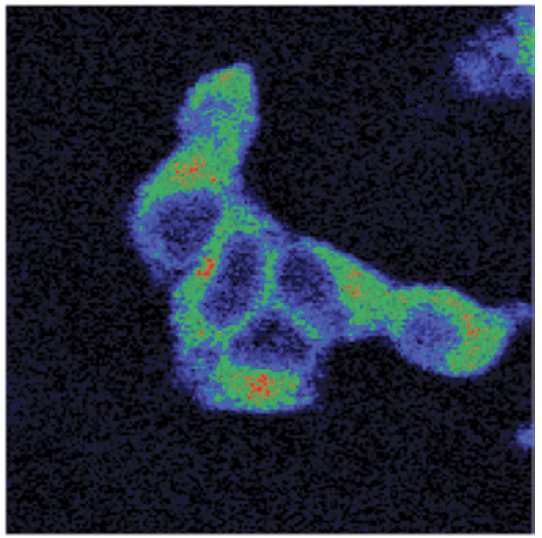

 J. Am. Chem. Soc. 132, 1194

Diagnosis: Detection of critical analytes

The sensor gives an optical response and is therefore functions as an optode. In a similar approach, ionophore based sensors composed of cryptaspherands with chromogenic substituents have been developed to detect alkali metals in blood serum

Kumar A et al (1988) Chromogenic ionophore-based methods for spectrophotometric assay of sodium and potassium in serum and plasma. Clin Chem 34:1709–1712

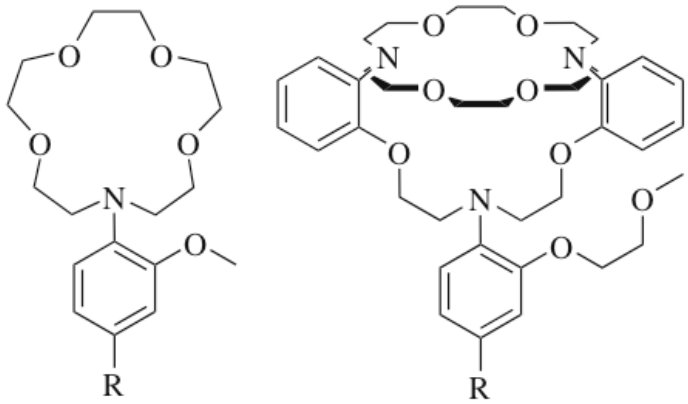

Na^+ sensor

K^+ sensor

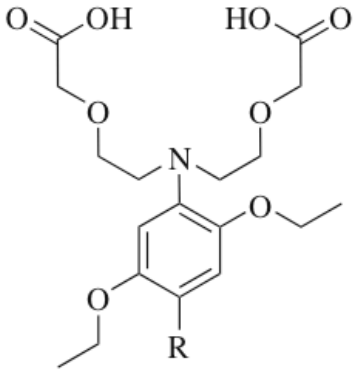

Ca^{2+} sensor

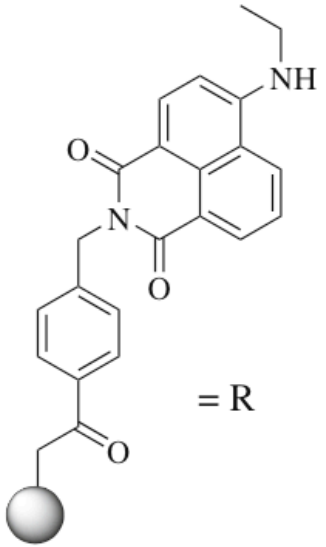

Diagnosis: Displacement essay

Piatek AM et al, *J Am Chem Soc* **126**, 6072

Threshold detection using indicator-displacement assays: An application in the analysis of malate in Pinot Noir grapes

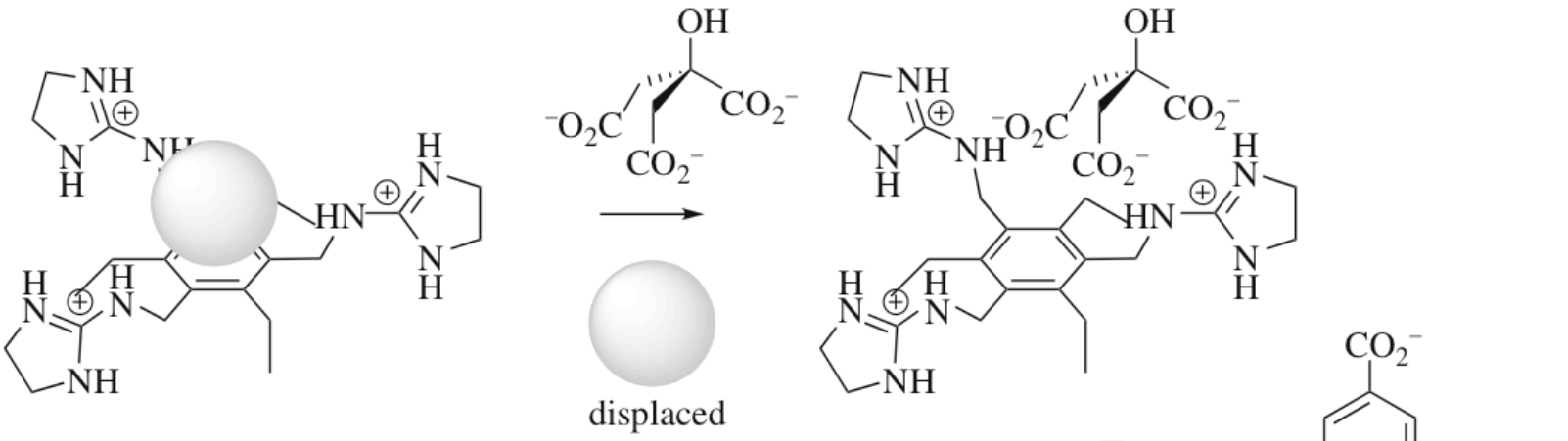

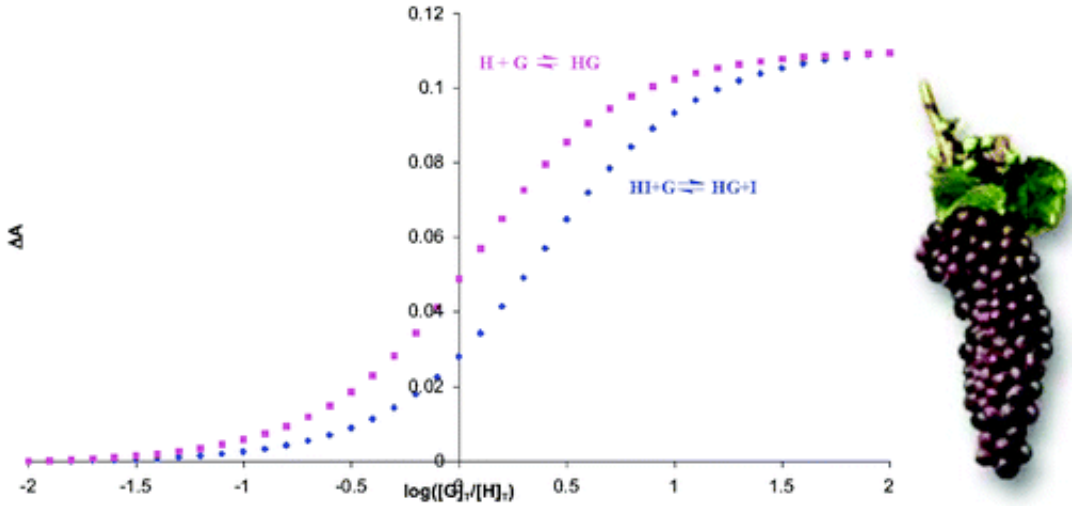

Diagnosis: Squaraine Dyes

Gassensmith JJ et al, *J Am Chem Soc*, **2007**, *129*, 15054

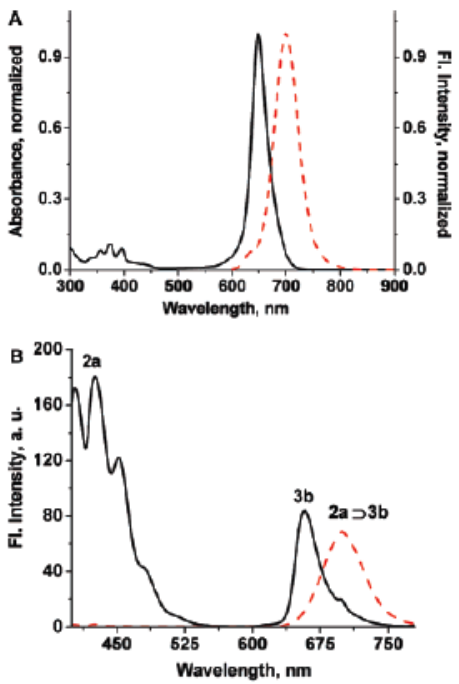

Figure 2. (A) Absorption (black full line) and fluorescence emission (red dashed line, ex: 580 nm) spectra for rotaxane **2a⊃3b** in chloroform. (B) Fluorescence emission spectra (ex: 350 nm) for an equimolar mixture of **2a** and **3b** (both 5 μM) (black full line) and a solution of **2a⊃3b** (red dashed line) in chloroform.

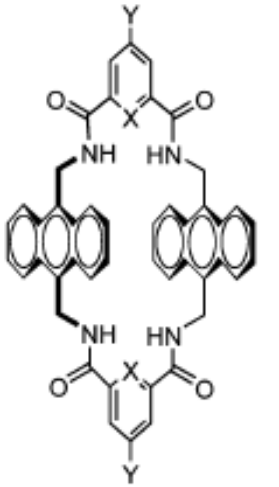

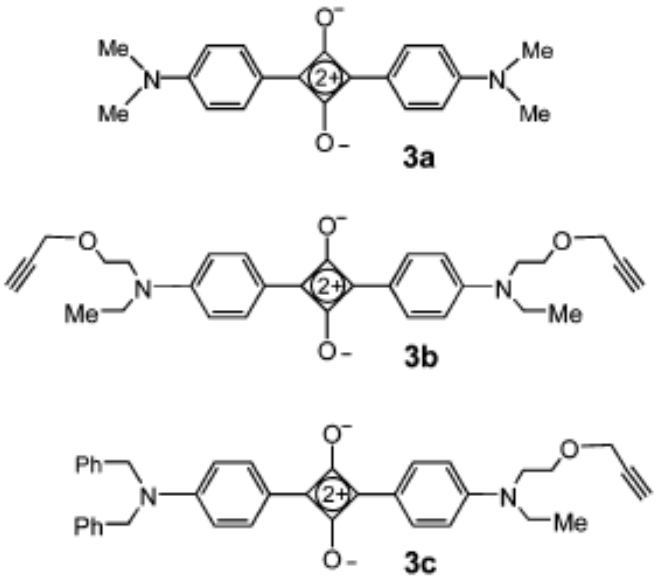

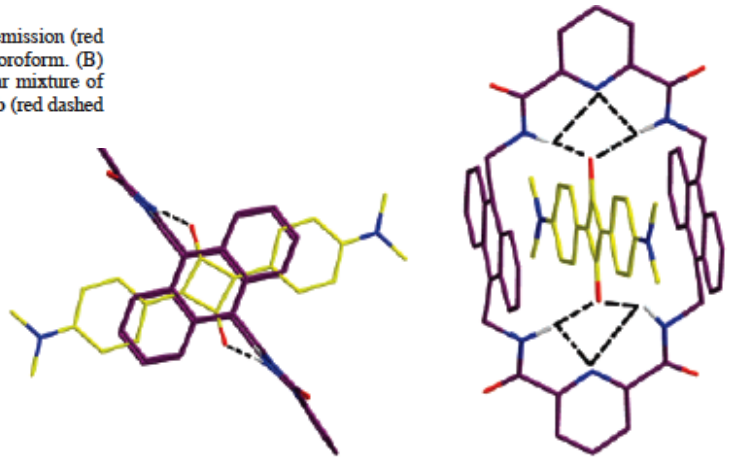

Figure 1. Two views of the X-ray crystal structure of **2a⊃3a**.

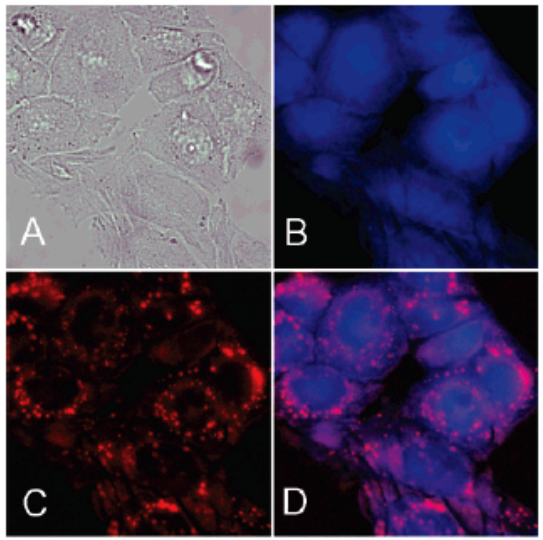

Figure 8. Fluorescence microscopy images of live CHO cells treated with separate aliquots of **3c** (10 μM) and **2b** (10 μM). Panel A: Phase contrast image. Panel B: Blue emission of uncomplexed **2b**. Panel C: Far-red emission of **2b⊃3c**. Panel D: Overlay of panels B and D.

Diagnosis: In Vivo Imaging

Fluorescents agents: lanthanides

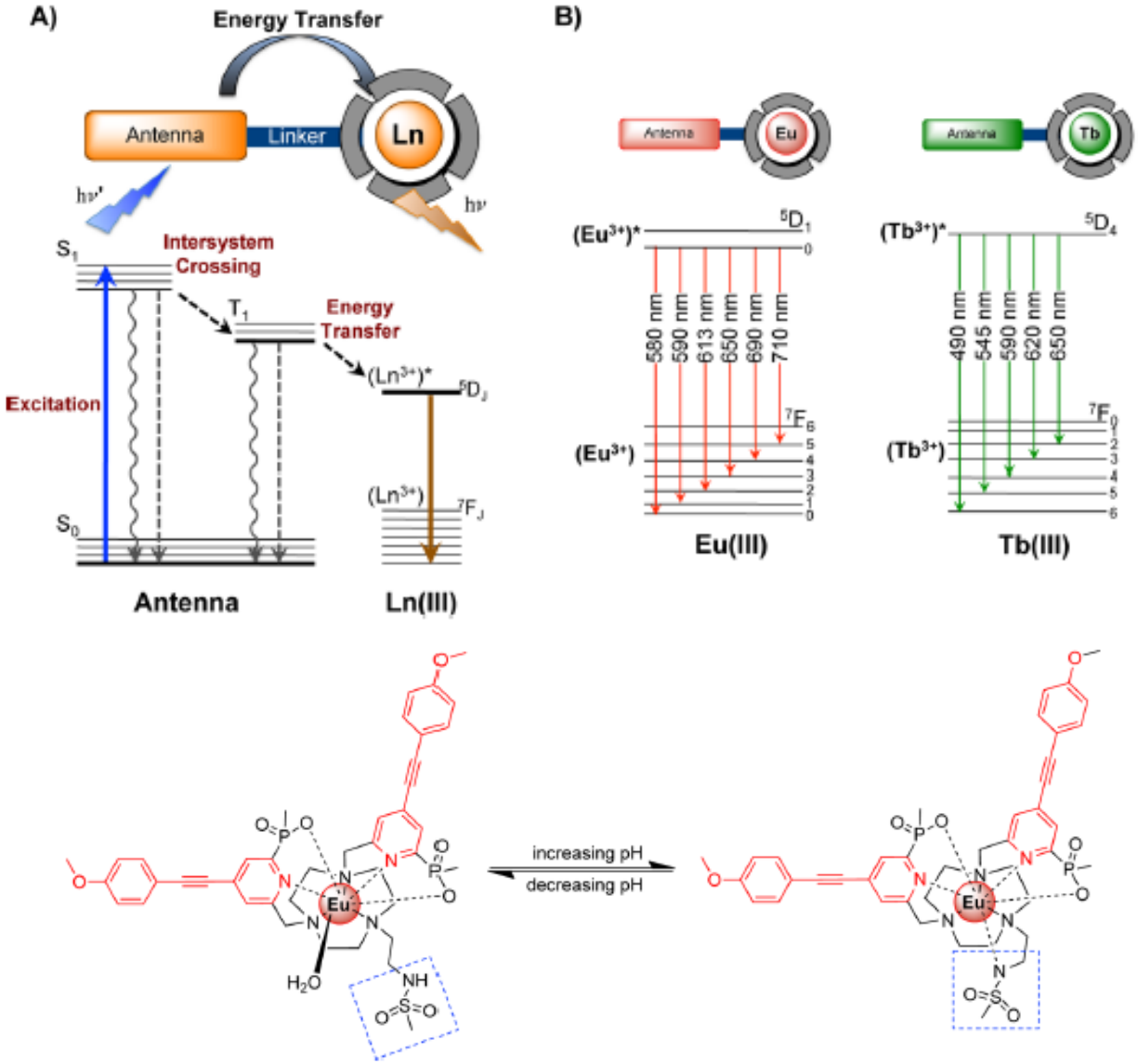

Parker et al. *Chem Commun*, **2008**, *131*, 434

Diagnosis: In Vivo Imaging

Fluorescents agents

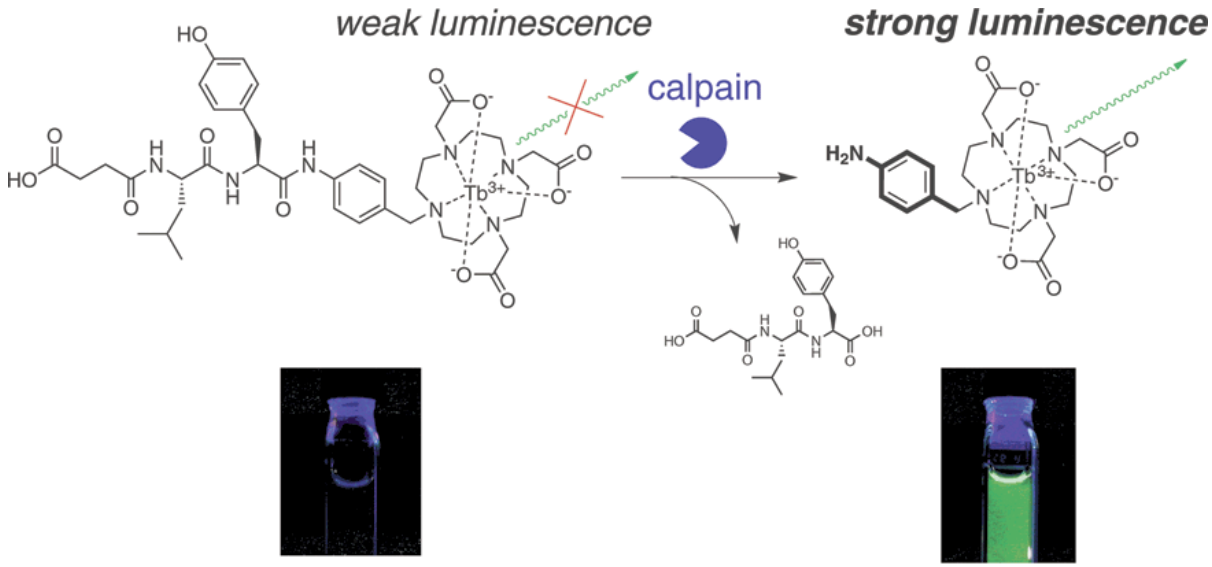

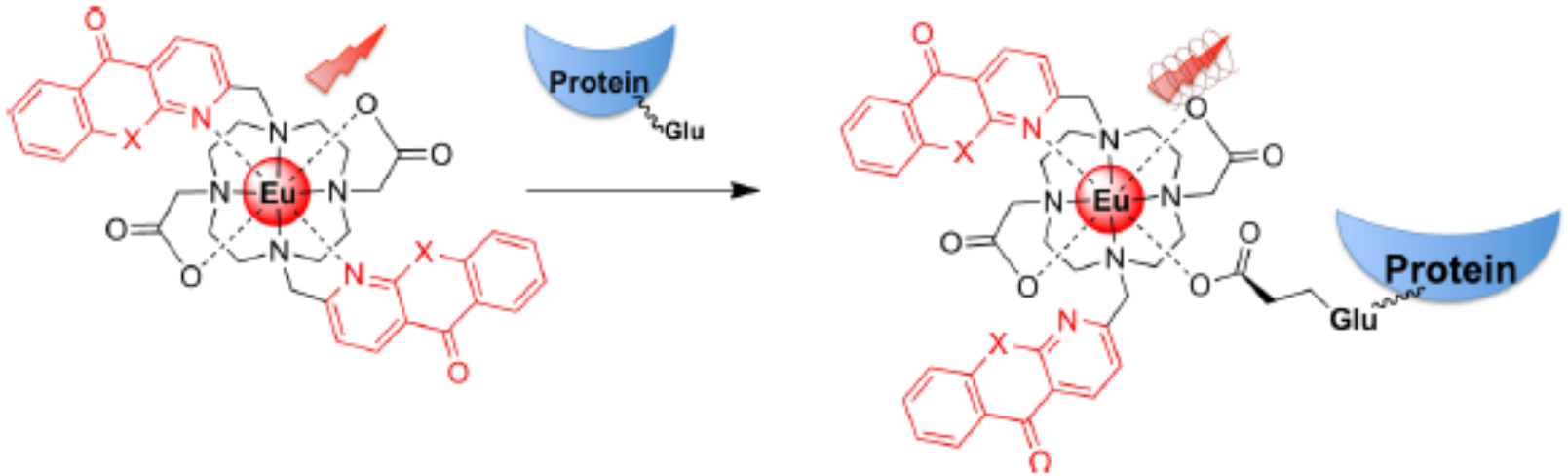

Peacock, *Dalton Trans.*, **2012**, *41*, 13154

Diagnosis: In Vivo Imaging
MRI Contrasts agents

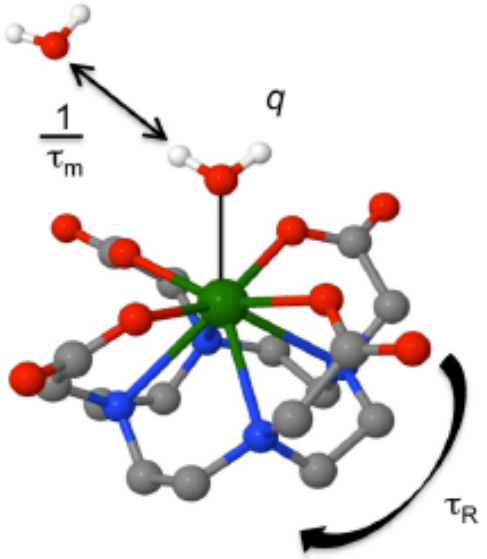

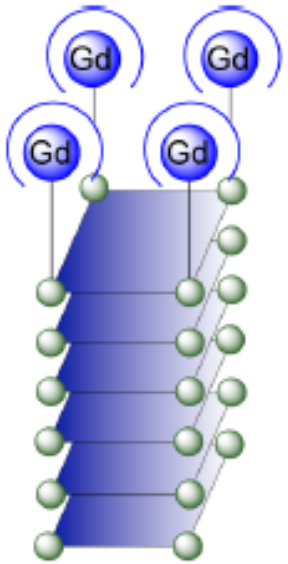

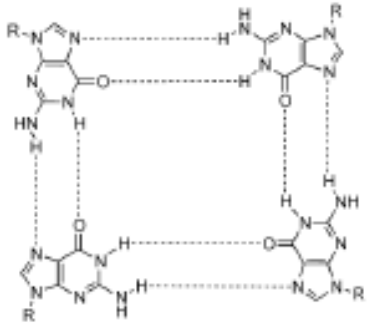

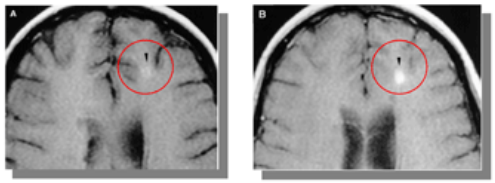

Visualization of a tumor before (A) and after (B) injection of contrast agent.

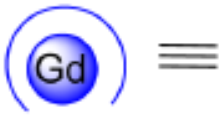

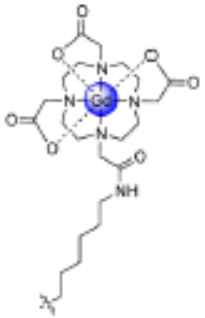

OR

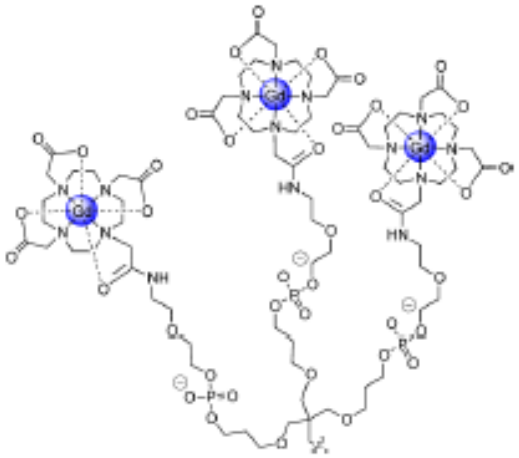

Parker, Dalton Trans., **2006**, 2757

Diagnosis: In Vivo Imaging
MRI Contrasts agents

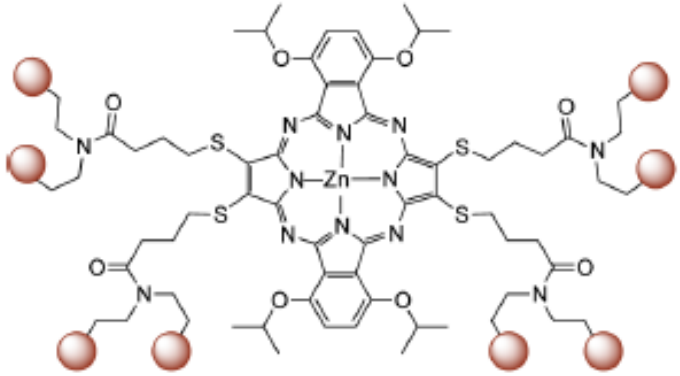

Zn-A_2B_2-8Gd(III)
r_1 = 12.8[A]

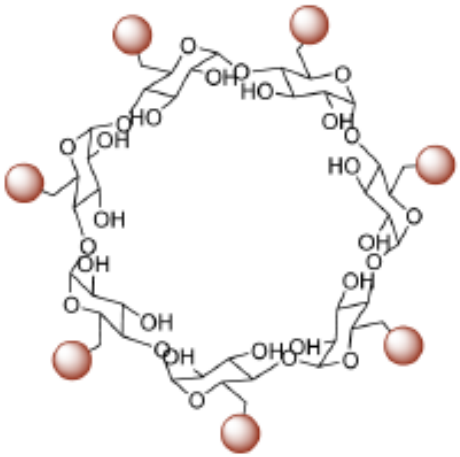

β-CD-Gd
r_1 = 12.2[B]

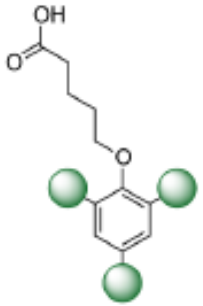

C3-Gd
r_1 = 15.4[C]

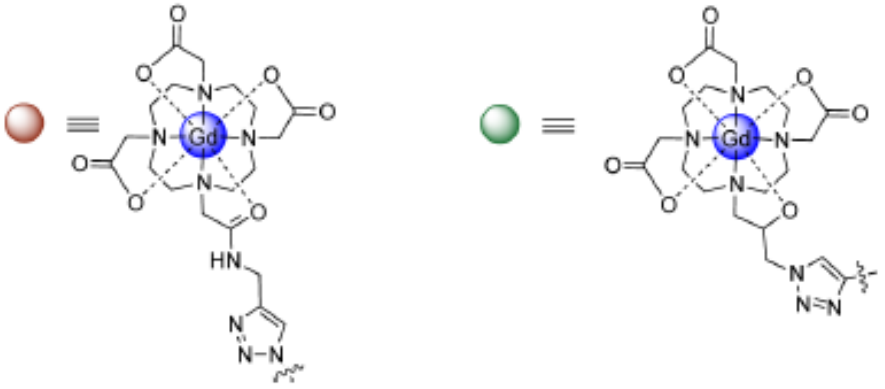

Nonat, *Inorg. Chem.*, **2009**, *48*, 4646

Diagnosis: In Vivo Imaging
MRI Contrasts agents

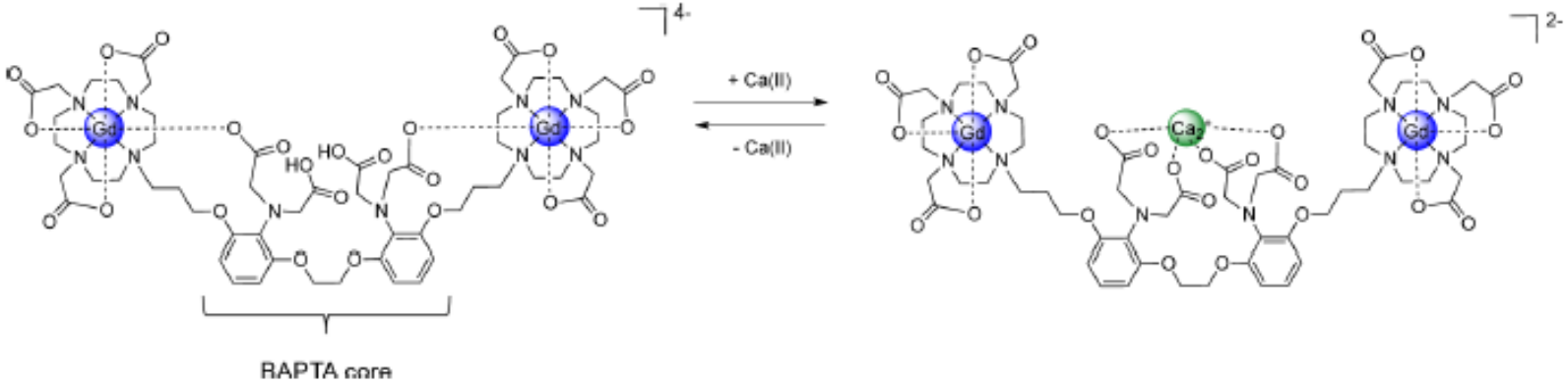

Meade, *J. Am. Chem. Soc.*, **1999**, *121*, 1413

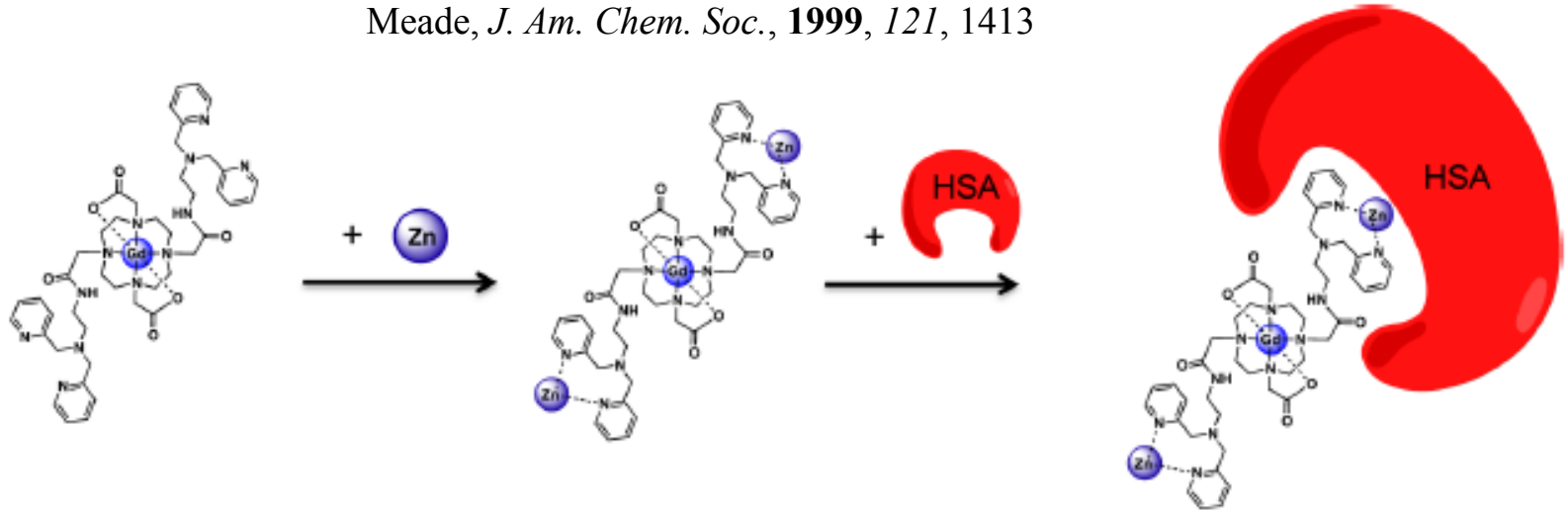

150% increase in r_1
(23 MHz)

Sherry, *J. Am. Chem. Soc.*, **2009**, *131*, 11387

Diagnosis: In Vivo Imaging
MRI Contrasts agents

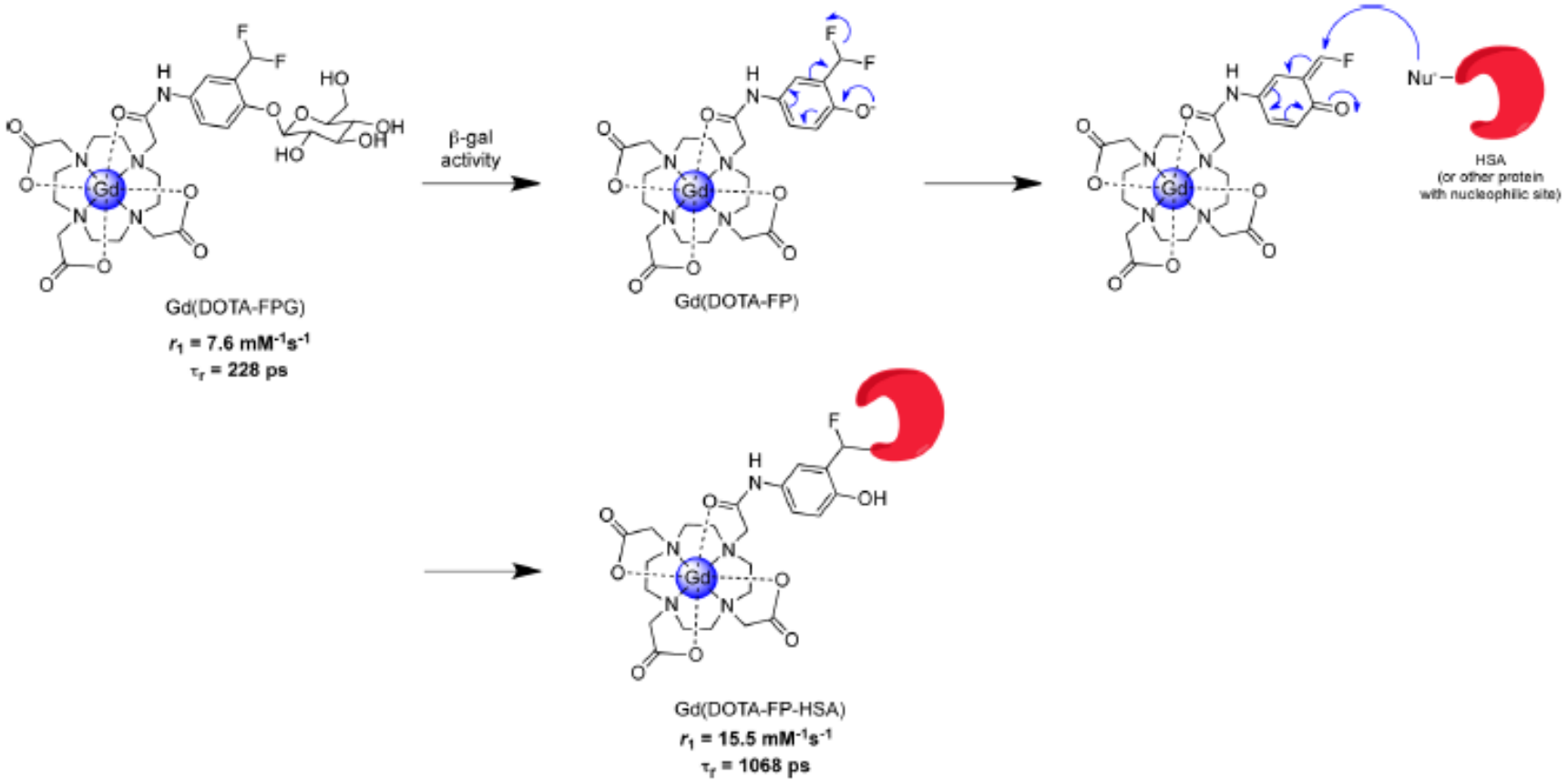

Chang, *Bioconjugate Chem.*, **2007**, *18*, 1716

Supramolecular Therapeutics

Chelation therapy

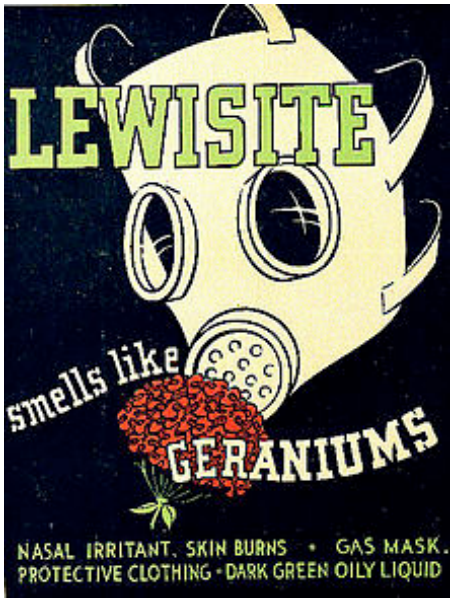

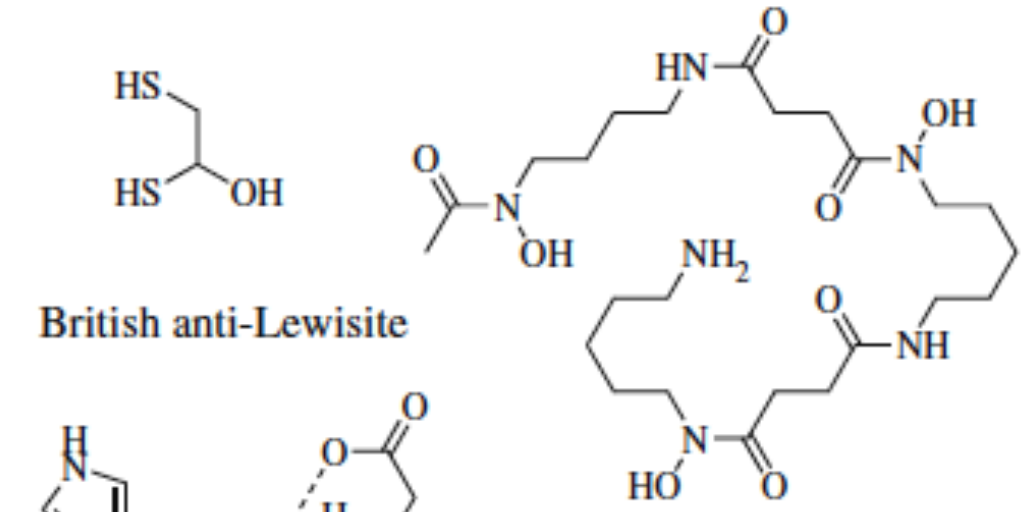

British anti-Lewisite

desferrioxamine

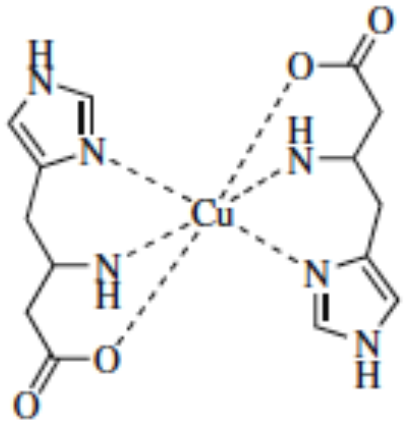

copper histidine complex

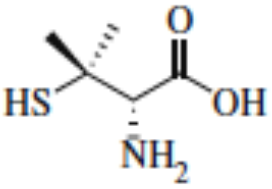

D-penicillamine

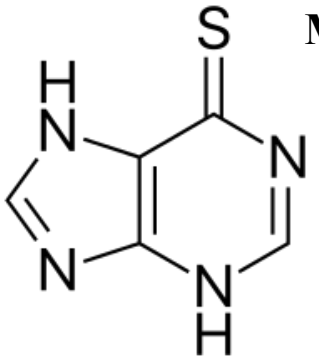

Mercaptopurine

Copper Imbalance: Wilson diseases

Chelation therapy

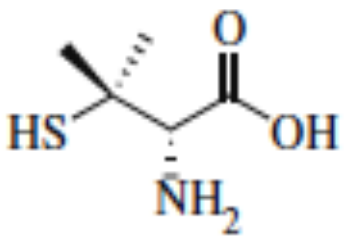

D-penicillamine

Wilson's disease or hepatolenticular degeneration is an autosomal recessive genetic disorder in which copper accumulates in tissues; this manifests as neurological or psychiatric symptoms and liver disease. It is treated with medication that reduces copper absorption or removes the excess copper from the body, but occasionally a liver transplant is required.

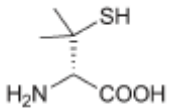

D-Pen

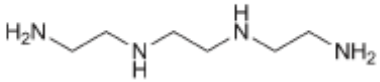

TETA

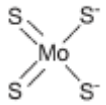

TTM

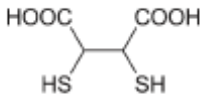

DMSA

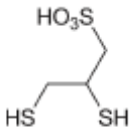

DMPS

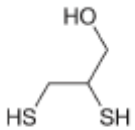

BAL

Tripodal pseudopeptides

H_3L^1: X = OEt
H_3L^2: X = NH_2
H_6L^3: X = OH

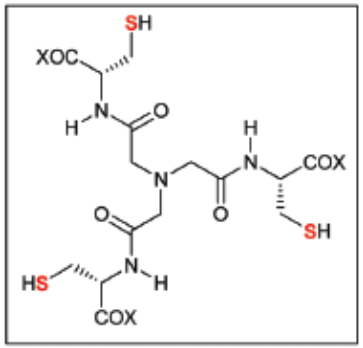

Delangle, Dalton Trans., **2012**, *41*, 6359

Supramolecular Therapeutics

Macrocyclic Complexes for Radiotherapy

^{90}Y, half time of 64h

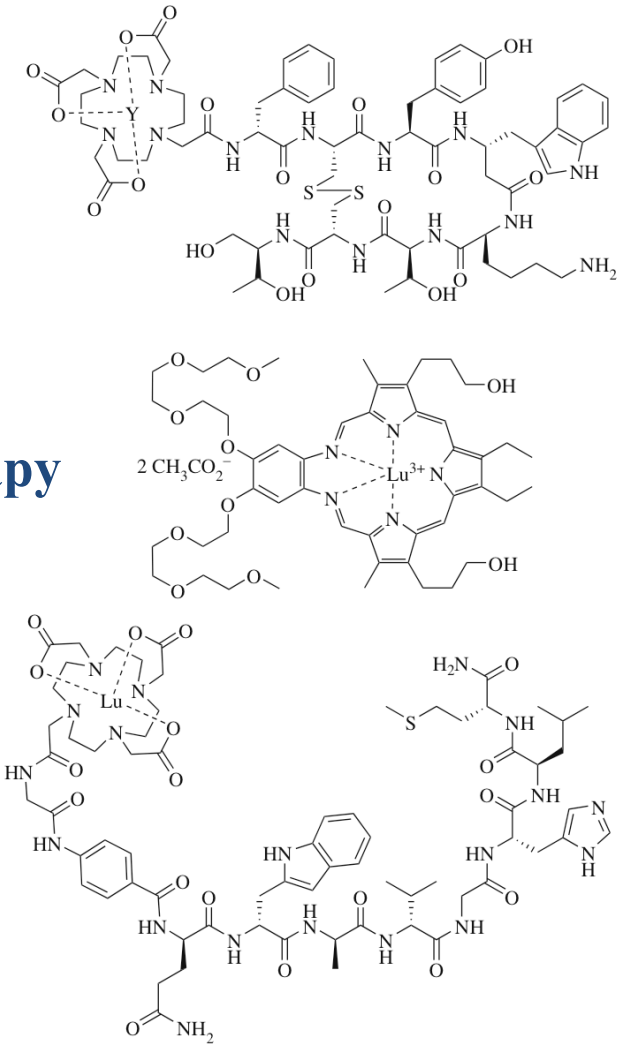

Photodynamic Therapy

porphyria

Fig. 7.3 Radiotherapeutics: (from *top*) DOTA—tyr3-octreotide, LUTRIN® and Lu-177-AMDA

Supramolecular Therapeutics

Photodynamic Therapy

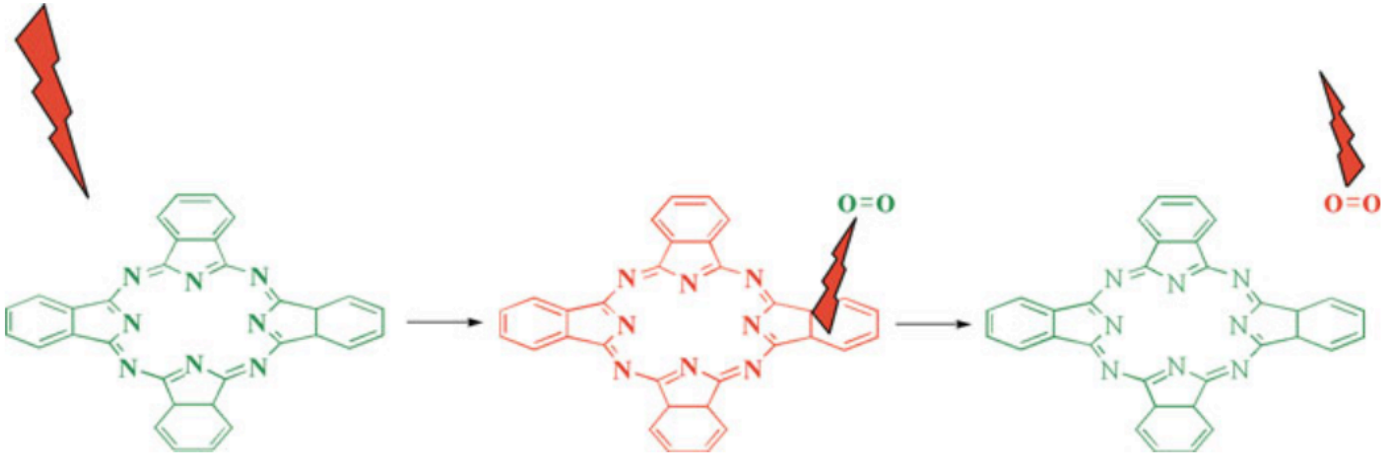

Fig. 7.4 Generation of therapeutic $^1O_2$ for photodynamic therapy

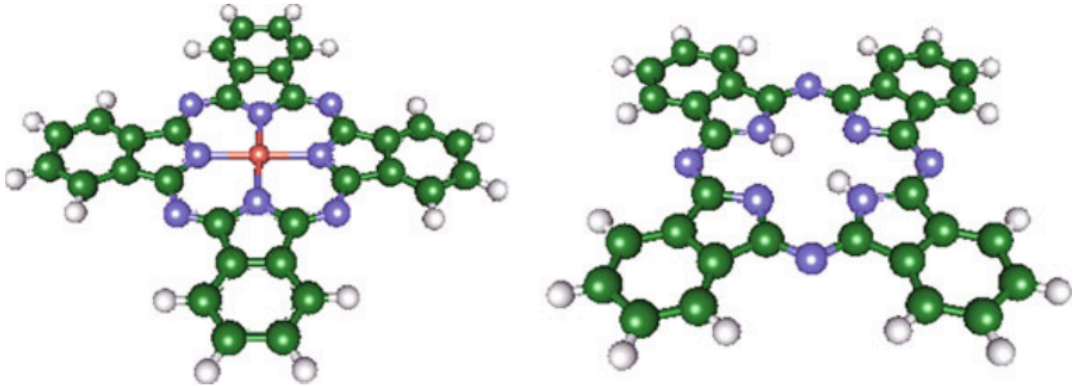

Fig. 7.5 Phthalocyanine crystal structures: a copper complex [12] (*left*) and the metal free macrocycle [13] (*right*)

Supramolecular Therapeutics

Texaphyrin

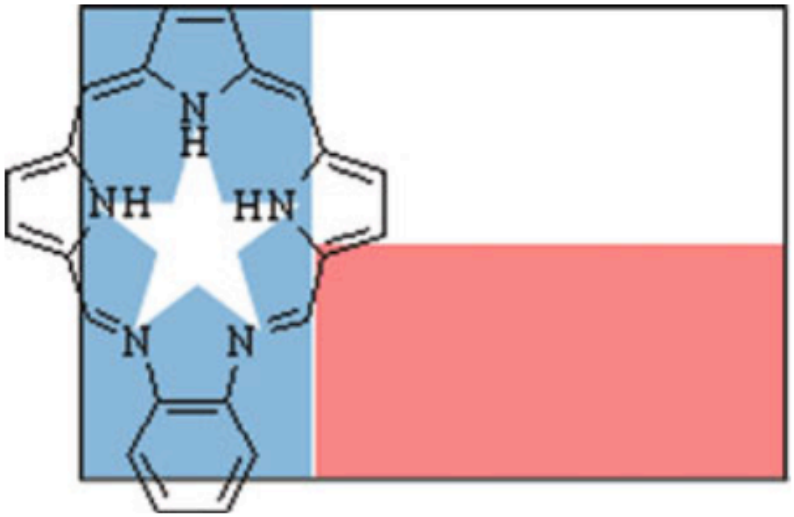

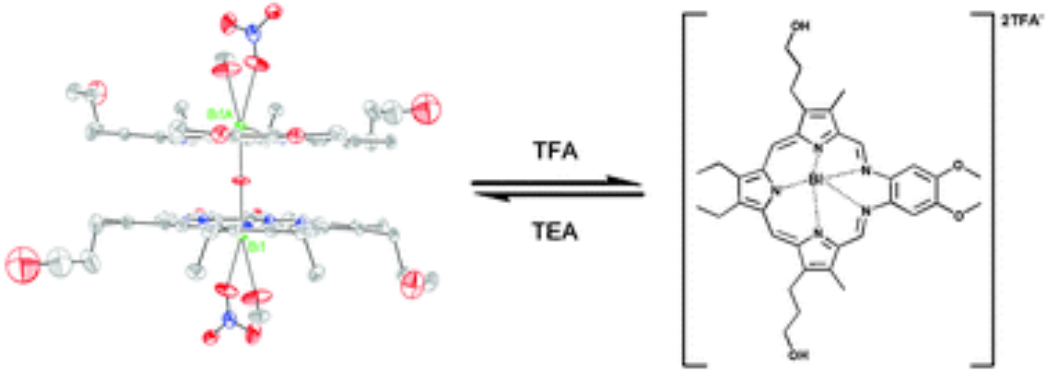

Sessler, *Chem. Commun.*, **2010**, 46, 7900

Sessler JL et al., Synthesis and structural characterization of lanthanide(III) texaphyrins., 1993, Inorg Chem 32, 3175

Sessler JL, Miller RA, Texaphyrins – New drugs with diverse clinical applications in radiation and photodynamic therapy. Biochem Pharmacol , 2002, 59:733

Drug Delivery and Controlled Release

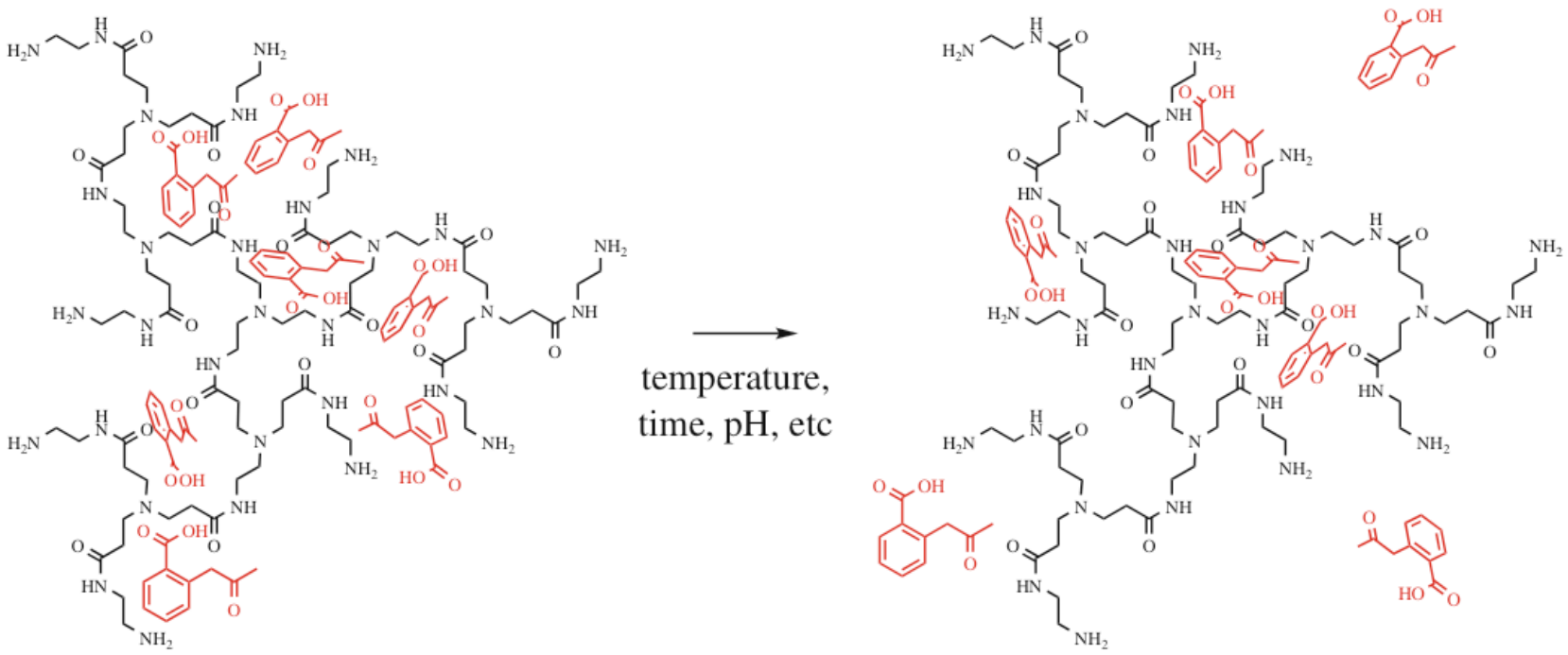

Fig. 7.8 Controlled release of therapeutic drugs by a dendrimer

Malik N, Evagorou EG, Duncan R (1999) Dendrimer-platinate: a novel approach to cancer chemotherapy. Anti-Cancer Drugs 10: 767–776

Padilla De Jesus OL et al (2002) Polyester dendritic systems for drug delivery applications: *in vitro* and *in vivo* evaluation. Bioconjug Chem 13:453–461

Cyclams as Anti-HIV Agents

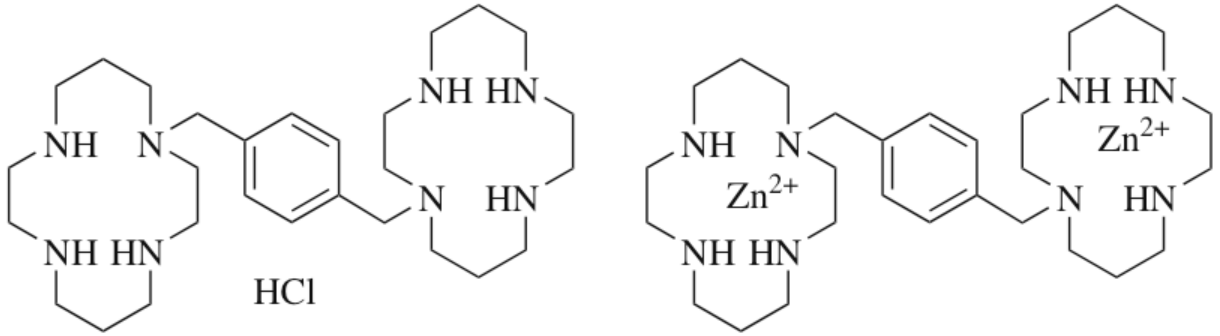

Fig. 7.9 Bis(cyclam)s with anti-HIV activity

Structure and dynamics of metallomacrocycles, Recognition of zinc xylyl-bicyclam by an HIV coreceptor.

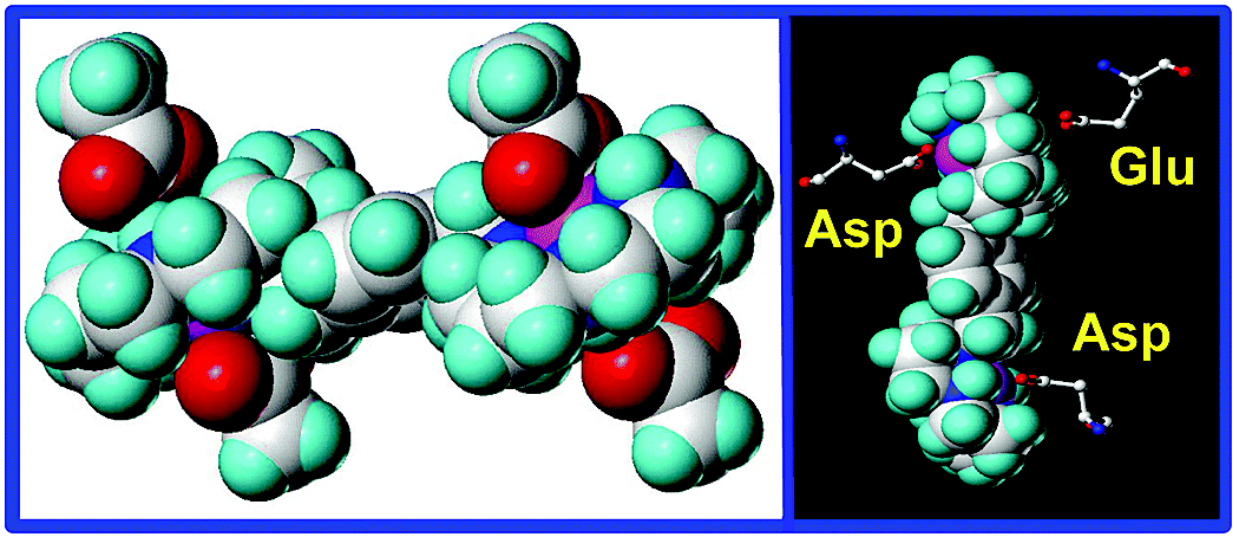

Liang XY et al, J Am Chem Soc, 2002, 124, 9105

A Supramolecular Solution to Alzheimer's Disease?

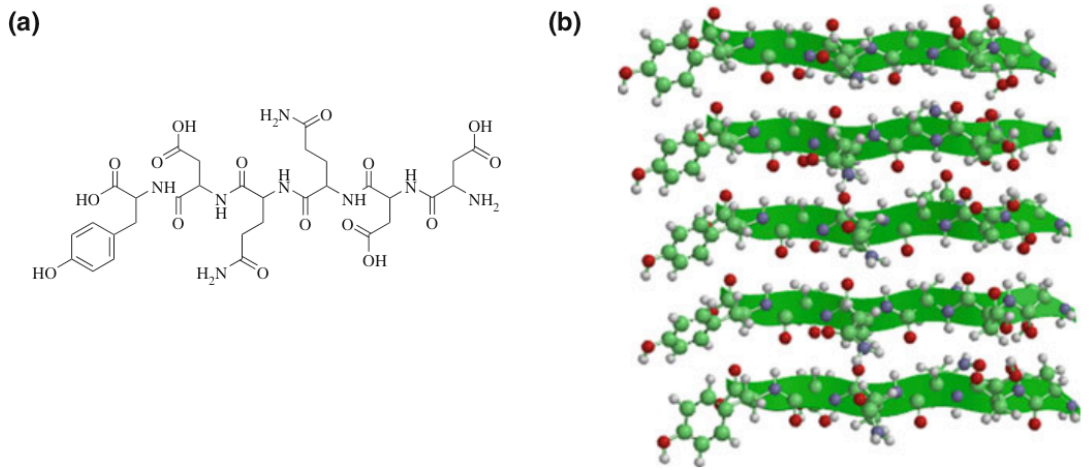

Fig. 7.10 The β-sheet structure formed by the NNQQNY sequence (**a**) in amyloid-β proteins that leads to plaque formation [30]

Fig. 7.11 A tetrahydrosalen-based therapy to target Alzheimer's disease [31]

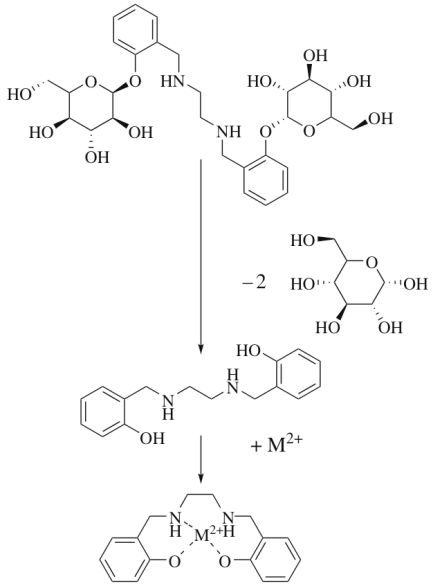

Goldschmidt L et al **(2010)** Identifying the amylome, proteins capable of forming amyloid- like fibrils. *Proc Natl Acad Sci USA* 107:3487–3492

Stor T et al **(2009)** Glycosylated tetrahydrosalens as multifunctional molecules for Alzheimer's therapy. *Dalton Trans* 3034–3043

Calixarenes as Therapeutic Agents

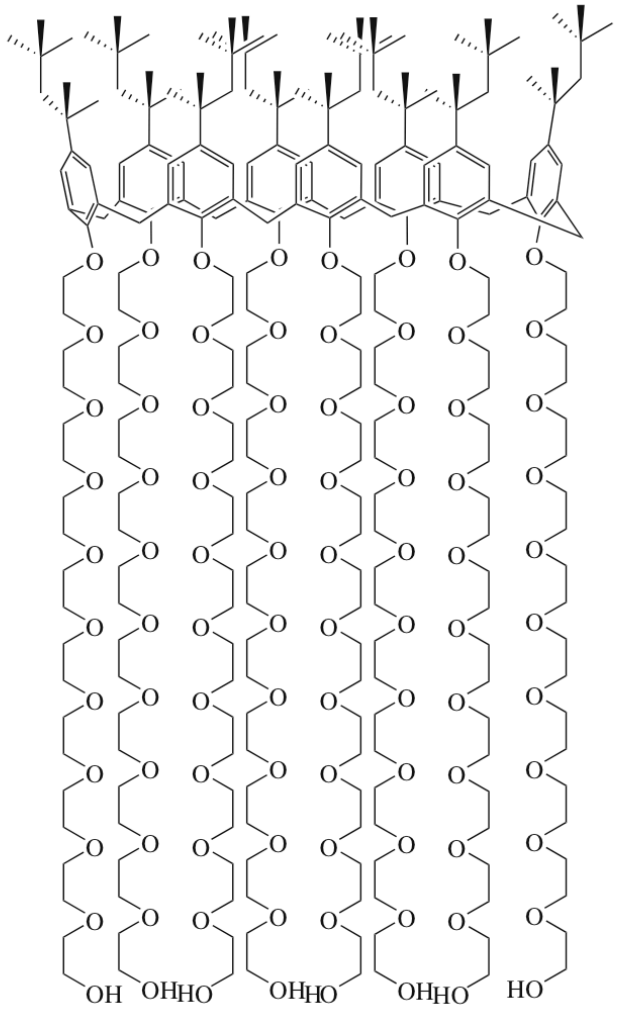

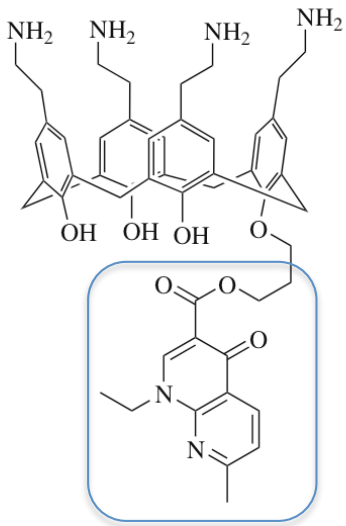

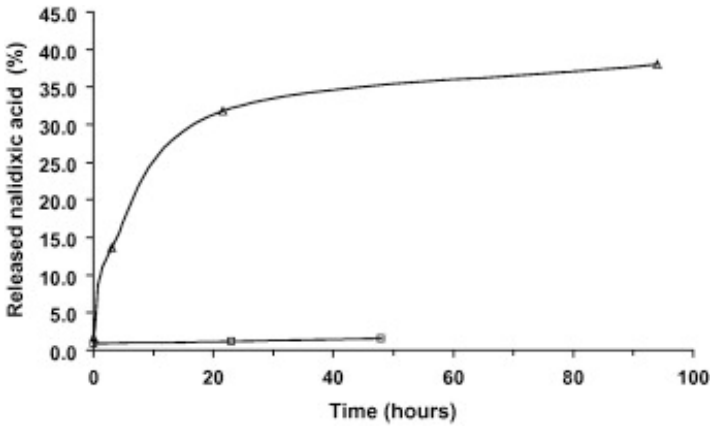

Diamba HM et al (2009) Towards calixarene-based prodrugs: drug release and antibacterial behaviour of a water-soluble nalidixic acid/calix[4]arene ester adduct. Bioorg Med Chem Lett 19:2679–2682

Fig. 7.12 Calixarene-based therapeutics: anti-tubercular *Macrocyclon* [32] (*left*) and a nalidixic acid delivering prodrug [34] (*right*)

Antitubercular agent, **1955**

Supramolecular Antibiotics

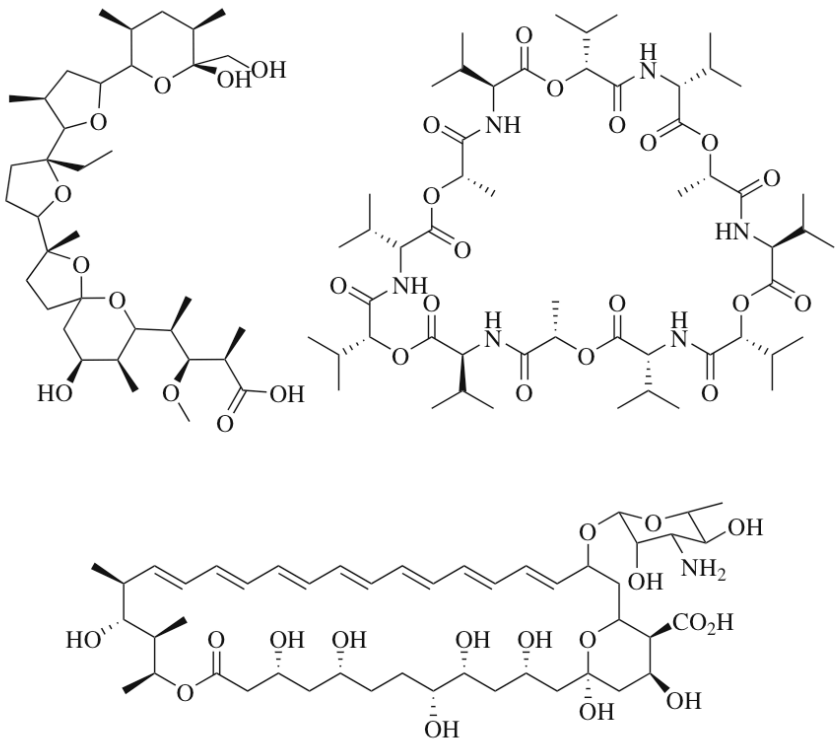

Fig. 7.13 Some naturally occurring antibiotics and related compounds: monensin (*top left*) valinomycin (*top right*) and amphotericin (*bottom*)

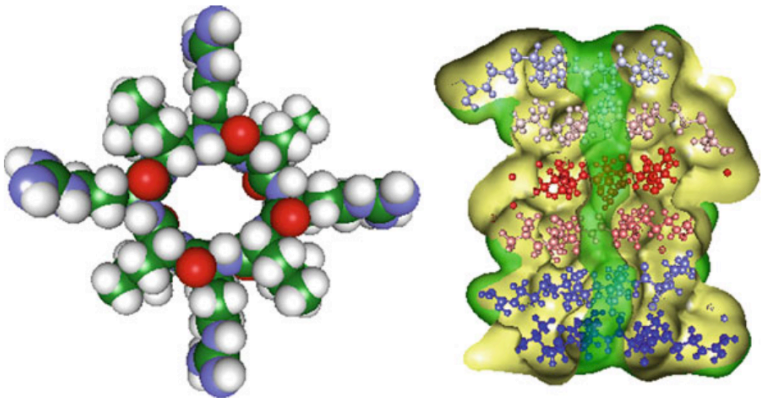

Fig. 7.14 Self-stacking cyclopeptides [36]

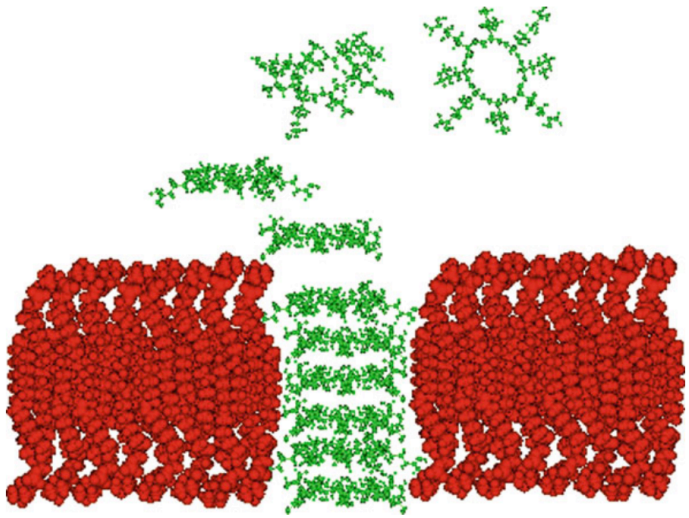

Fig. 7.15 Proposed mode of antibiotic action by cyclopeptides: tubes (*green*) form and aggregate to disrupt bacterial membranes (*red*)

Fernandez-Lopez S et al **(2001)** Antibacterial agents based on the cyclic D,L-α-peptide architecture. *Nature* 412:452–455

Ruzin A et al **(2004)** Mechanism of action of the mannopeptimycins, a novel class of glycopeptide antibiotics active against vancomycin-resistant gram-positive bacteria. *Antimicrob Agents Ch* 48:728–738

Motiei L et al **(2009)** Antibacterial cyclic D,L-alpha-glycopeptides. *Chem Commun* 3693–3695